UNIVERSITY OF CALIFORNIA,

IRVINE

Characterization of Local Conformational Structure and Mechanical Properties of Chromatin using Fluorescence Lifetime Imaging Microscopy and Phasor Analysis

THESIS

Submitted in partial satisfaction of the requirements

For the degree of

MASTER OF SCIENCE

in

Biomedical Engineering

by

Persia F Goudarzi

Thesis Committee:

Associate Professor Michelle Digman, Chair

Professor Enrico Gratton

Assistant Professor Daryl Preece

2021

TABLE OF CONTENTS

LIST OF FIGURES

LIST OF TABLES

ABSTRACT OF THE THESIS

Characterization of Local Conformational Structure and Mechanical Properties of Chromatin using Fluorescence Lifetime Imaging Microscopy and Phasor Analysis

By

Persia Goudarzi

Master of Science in Biomedical Engineering

University of California, Irvine, 2021

Associate Professor Michelle Digman, Chair

Chromatin is a complex of macromolecules that plays a very important role in packaging the long strand of DNA inside the eukaryotic nucleus. Chromatin enables and regulates many DNA functions and interactions with other molecules including DNA transcription, replication, and repair. During the cell division, chromatin ensures proper division and transfer of the genetic material to daughter cells. To fulfill these roles, chromatin must constantly undergo reconfiguration and reorganization of its structure. Therefore, local conformational structure and mechanical properties of chromatin play a crucial role in creating the highly dynamic structure of chromatin. Furthermore, recent studies link mechanobiology of the nucleus, specifically nuclear stiffness and deformability, to cancer metastasis. Due to the fact that chromatin structure is highly compact and dynamic, visualizing and studying its structure, remodeling and mechanical properties is very difficult. In this research, we showed that Fluorescence Lifetime Imaging Microscopy (FLIM) and phasor analysis can be used as a powerful technique to study local conformational structure and mechanical properties of chromatin during mitotic cell division and in metastatic tumor cells. More specifically, the findings from the lifetime values revealed

information about the size, stiffness, deformability, and accessibility of the minor grooves in chromatin. The findings from this study confirmed significant structural differences between metaphase and interphase chromatin, but they also revealed significant variations within chromatin at any stage. We postulated that these variations are largely sequence dependent. Two types of regions with distinct conformational and mechanical properties were identified in chromatin. One of them had a significantly longer lifetime which was indicative of more rigid and larger binding area. These regions were attributed to GC-rich minor grooves. The other regions with significantly shorter lifetime, indicating softer and smaller binding sites, were associated with AT-rich minor grooves. Moreover, the lifetime of metaphase and interphase chromatin differed more significantly in GC-associated grooves. Therefore, we concluded that there were far more AT-rich minor grooves accessible for binding in both metaphase and interphase chromatin to the extent that the effect of chromatin condensation during metaphase did not cause very significant differences in the lifetime values. Finally, the fluorescence lifetime analysis revealed that chromatin in highly aggressive metastatic tumors like MB231 and MFC7 was significantly softer and more deformable than non-tumorigenic cells like MCF10A. There was a correlation between softness and deformability of chromatin and the metastatic aggressiveness of the tumors.

Chapter One: Chromatin Structure and Function

1.1. What is chromatin

Chromatin is a complex of macromolecules composed of DNA and proteins that form chromosomes in the nucleus of eukaryotic cells (1). It is how eukaryotic cells store and transfer their genetic instructions for life. Understanding the architecture and function of chromatin structure, therefore, is key in understanding how eukaryotic cells form, develop, and grow and finally differentiate and pass along their hereditary information. Each human cell has a total of 6 billion base pairs of DNA and each base pair is about 0.34 nanometers long. Therefore, each cell must fit in its nucleus approximately 2 meters of DNA (2). The human body has an estimated 50 trillion cells and that makes a total of 100 trillion meters of DNA in the human body—that is roughly 600 times the distance from Earth to the Sun (2). Chromatin's primary function is to compact this large amount of DNA into the eukaryotic nucleus and the body they make up. This is possible because chromosomal DNA wraps around certain proteins and condenses to fit inside the cell. The major proteins in chromatin are histones, which function as packaging elements for DNA to compact itself into a form that fits in the cell nucleus (3). These proteins provide energy in the form of electrostatic interactions to fold DNA into packages that are much smaller than the DNA volume itself. Since histones are positively charged proteins and DNA is negatively charged, they strongly bind together inside microscopic nuclei (2). The resulting complex of DNA and histones is called chromatin. Any transcriptional activity or cellular events that occurs in the nucleus is directly or indirectly regulated by the characteristic of the chromatin structure (4). Therefore, the assembly and nature of chromatin structure play a fundamental role in cellular development, identity, and fate.

1.1. Chromatin Structure

The structure of chromatin depends on the stage of the cell cycle. Chromatin comprises basic functional and structural repeating units called nucleosome. Nucleosome is an assembly of DNA and histones. A Long array of nucleosome tightly folds to create chromatin fiber. Chromatin fiber undergoes further compaction and condensation during cell division creating chromosomal structures to transfer genetic information to the daughter cells. The most astonishing characteristic of a chromosome is the length of the DNA that is packaged into it. There are over 3 billion base pairs of DNAs in the human genome, which are stored in a nucleus of only 10 μm (4). Each nucleosome contains 146 base pairs of DNA wrapped 1.65 times around eight histone proteins. An additional histone wrapped with another 20 base pairs of DNA, called linker DNA, joins the histone octamer in the nucleosome resulting in two full turns of DNA around the histone core to form a structure called chromatosome. Formation of nucleosomes shortens the length of DNA from 1 meter long to 14 centimeters (2). However, DNA needs to undergo further compaction and packaging to fit into a cell nucleus.

Nucleosomes fold up to form a shorter and thicker fiber approximately 30 nm in diameter called chromatin fiber. This fiber loops into 300 nm-long structures which are compressed and folded to form a 250 nm-wide fiber tightly coiled and condensed into higher order structures called chromatids (2). After DNA replication, two identical sister chromatids joined at the centromere form a duplicated chromosome. During mitosis, each chromatid of a chromosome is transferred to each of the two daughter cells. To achieve the equal partitioning of the genetic material, the genomic DNA is highly condensed into metaphase chromosomes. The chromosomes during metaphase are 10,000 times more condensed compared to a naked strand of DNA (2). This level of compaction is due to chromatin fibers' ability to repeatedly fold to form

higher order structures. Once the process of cell division is complete and two daughter cells are formed, chromosomes decondense again into chromatins. Exactly how this dramatic condensation and de-condensation of chromatin are achieved as cells transition between different phases of the cell cycle is one of the key challenges in structural biology. Figure 1 is an illustration of chromatin organization and different structural orders.

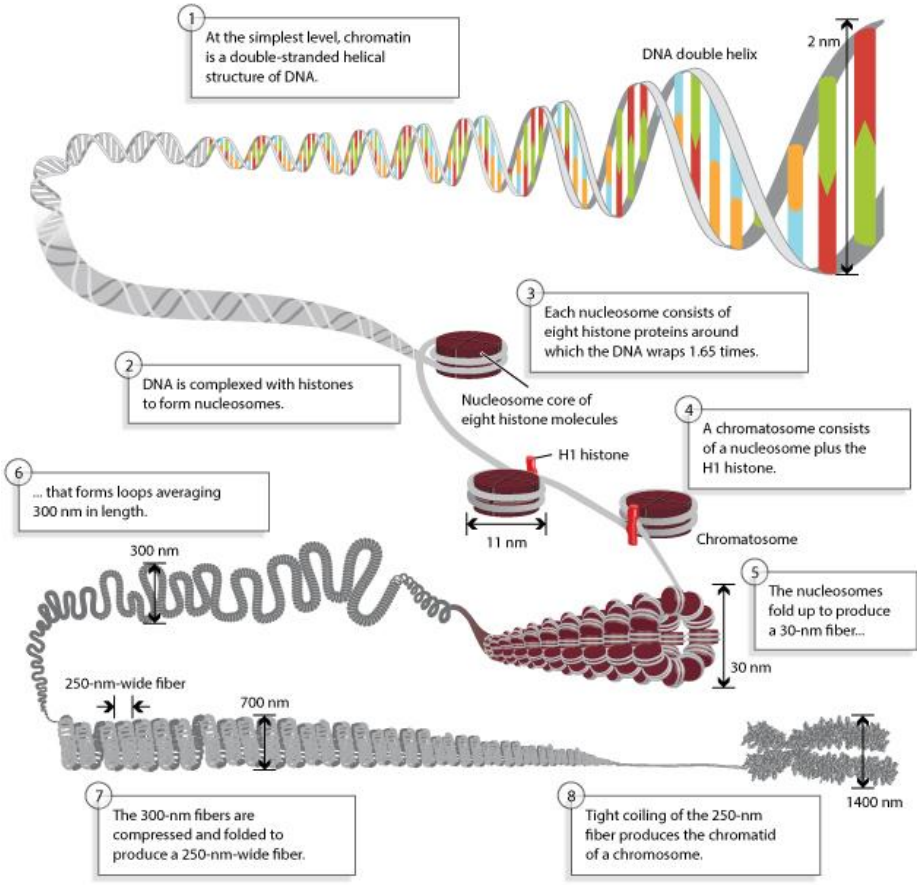

Figure 1: Schematic representation of chromatin structure at different organizations and structural order *(2)*.

1.2. DNA Structure

Deoxyribonucleic acid is a double helix molecule made up of two antiparallel polynucleotide chains. There are four types of nitrogenous nucleic acid bases or nucleotides in the DNA:

adenine, thymine, cytosine, and guanine. Base adenine (A) always pairs with thymine (T) and base guanine (G) pairs with cytosine (C). Figure 2 shows a schematic illustration of the double helix polynucleotide chains attached together by the base pairs.

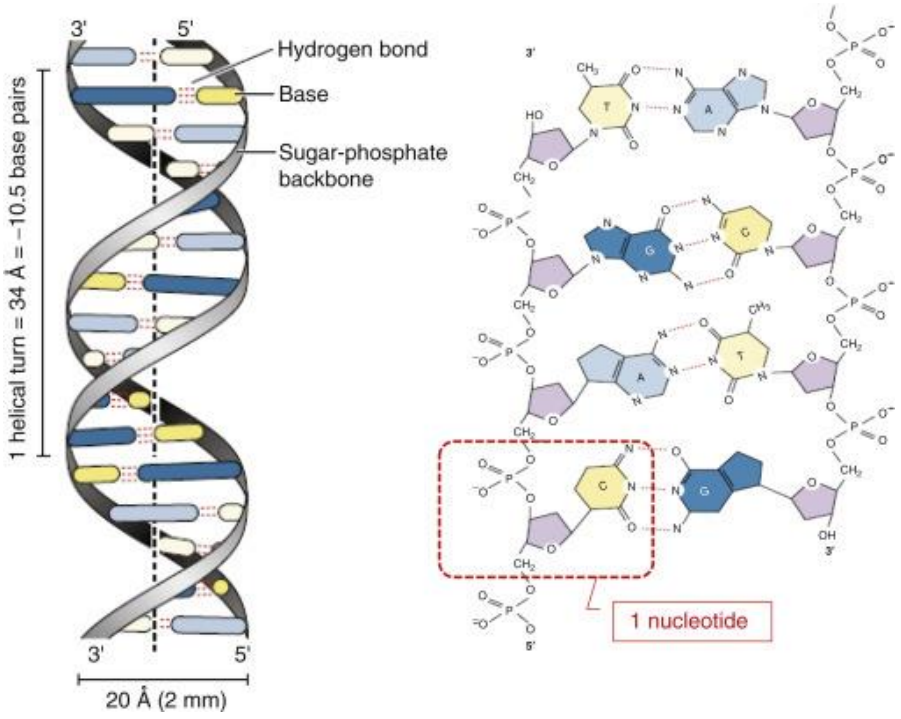

Figure 2: Schematic illustration of the structure of deoxyribonucleic acid *(5)*.

Hydrogen bonding between these bases holds the two antiparallel polynucleotide chains together (4). Another force that holds the DNA together is the Vander Waals force causing the hydrophobic stacking interactions between base pairs. The hydrogen bonds and hydrophobic stacking interactions stabilize the two antiparallel polynucleotide chains forming the DNA (4). Figure 3 illustrates the hydrogen bonding paring base A to T and base G to C as well as hydrophobic base stacking between A-T and G-C pairs.

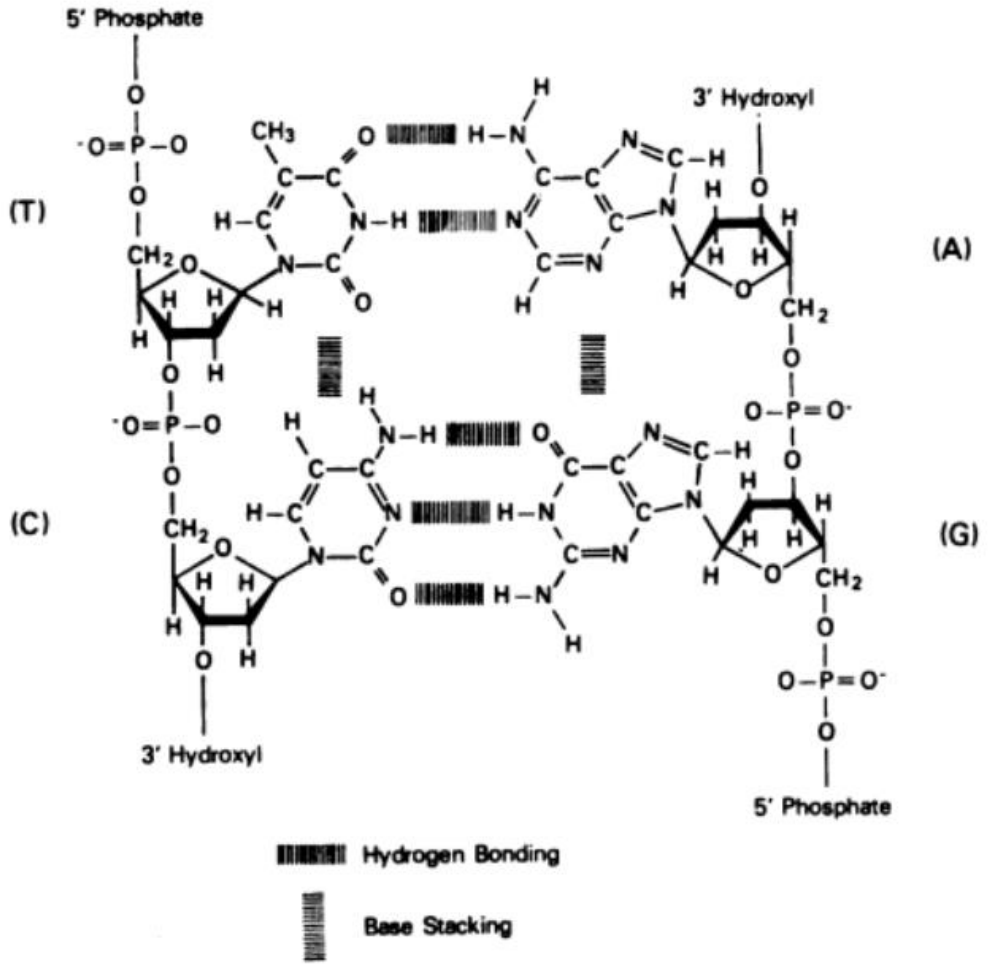

Figure 3: Hydrogen Bonding and Hydrophobic Base Stacking interactions stabilize the polynucleotide chains *(4)*.

Since the stability of the polynucleotide chains depends on the interactions between nucleotide bases, the DNA sequence determines the geometry and stability of the bonds and stackings (6). Ultimately, the DNA sequence significantly influences conformation of the DNA structure and properties of the double helix (4). The DNA structure under normal conditions of physiological ionic strength is a regular helix that turns every 3.4 nm and has 10.5 base pairs per turn (4). This structure is known as B-DNA. Every base pair of B-DNA rotates approximately 34° relative to the previous base twisting the two polynucleotide chains around each other and

creating a right-handed double helix with minor grooves and major grooves. A major groove is approximately 2.2 nm while a minor groove is around 1.2 nm across (7). Figure 4 shows a schematic of the twisting and turns of the polynucleotides creating the DNA double helix and its major and minor grooves. The geometry of these grooves is largely sequence-dependent and is crucial in determining DNA functions and interactions with proteins (4) (7).

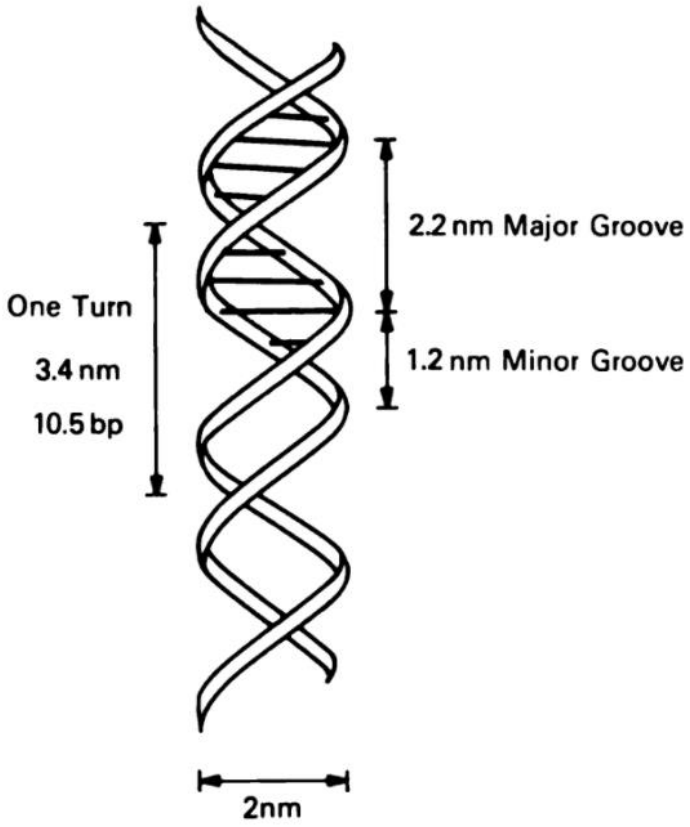

Figure 4: Schematic representation of twisted polynucleotide chains creating a double helix with minor and major grooves *(4).*

Adding to the complexity is the fact that this structure is not stiff and static. It is a deformable, dynamic structure with high energy existing naturally in it. DNA structure undergoes drastic conformational and structural changes like a spring that can be stretched and

compressed (8). These alterations occur periodically by normal cell functions during the cell cycle. DNA sequence and DNA-protein interactions are among the factors that determine conformation and properties of the double helix and alter the structure of DNA.

When it comes to the geometry stability of DNA structure, regions with base paring between guanine and cytosine, GC and CG base pairs, form stronger and more stable base stackings compared to adenine and thymine, AT and TA base pairs (6). It is because the hydrophobic stacking of T and A base pairs is weaker than G and C base pairs. Therefore, the polynucleotide chains have more stable geometry in regions rich in guanine and cytosine and the geometry of DNA structure is more deformable in regions with AT and TA base pairs. Moreover, GC base pairs are more tightly bound than CG base pairs, and AT base pairs are more tightly bound than TA base pairs. It is because GC pairs have higher stacking free energy than CG and AT pairs have higher stacking free energy than TA (6). Therefore, DNA local structure in order of increasing stability of the geometry and decreasing deformability is as follows: TA base pairs < AT base pairs < CG base pairs < GC base pairs. Conformationally, the most deformable and least stable regions are the TA-rich regions, and least deformable and most stable regions are the GC-rich regions.

Another conformational property of DNA structure strongly influenced by DNA sequence is the geometry of major and minor grooves. The structure and variations in structure of the DNA minor and major grooves are central in DNA-protein complexes and interactions (7). The DNA minor grooves have higher variability of dimensions and more easily become narrow or wide under different conditions. While the major grooves' dimensions change less often because they are energetically costly to distort (7). AT-rich regions of DNA tend to have very narrow minor grooves (7). The narrow geometry of these grooves is linked to enhanced negative

electrostatic potential, which is the mechanism by which proteins can penetrate inside these narrow minor grooves (7). While AT tracts are associated with narrowing of the minor grooves, TpA steps and GC base pairs tend to widen the minor grooves (9). Additionally, BII phosphate groups modulate width and depth of the grooves, a high density of BII phosphates creating wide and deep minor grooves and shallow major grooves (7). Figure 5 depicts the effect of BII phosphate groups on the width and depth of the minor and major grooves. The top left structure is the DNA segment with phosphate group BI with a narrow minor groove while the top right shows the widening of the minor groove in the presence of BII. Similarly, the bottom left shows a deep major groove in the presence of BI and a shallow major groove in a BII-rich segment of the DNA.

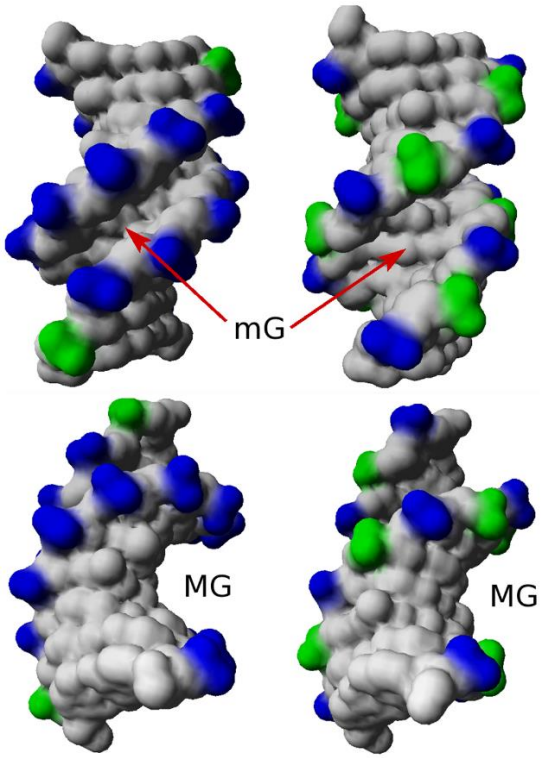

Figure 5: Narrow vs wide, shallow vs deep in minor grooves (top) and major grooves (bottom). Blue structures are BI phosphate groups and green structures are BII *(7)*.

1.3. Nucleosomal Structure

DNA structure twists into two supercoils each approximately 70 amino acids creating a superhelix containing about 146 base pairs of DNA (10). This highly distorted supercoiled DNA is called chromatomsome. Chromatosomes are the core of nucleosomes, yet they often are referred to as the nucleosome. However, the nucleosome consists of a chromatosome and a linker histone that facilitates the association of core nucleosomes with each other (11). Nucleosome is the fundamental repeating unit of chromatin in all eukaryotic cells. It consists of an octamer containing two copies of histone proteins H2A, H2B, H3 and H4 wrapping 146 DNA base pairs in 1.65 supercoiled, superhelical turns, as shown in Figure *6* (12).

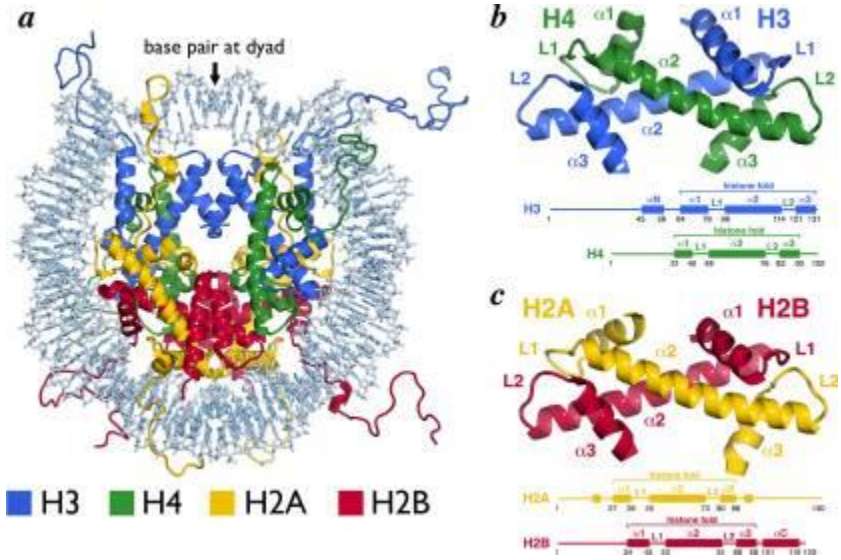

Figure 6: Nucleosome core structure and the histone-folded heterodimers forming the octamer *(11)*.

The highly distorted architecture of nucleosome is different from free DNA in that it is highly confined and occluded by both DNA strands and the histone octamer due to tight periodic interactions at 14 independent sites (12). These 14 regions are the sites of contact between the

minor grooves and the histones in DNA. Figure 7 shows a schematic of one-half of the nucleosomal DNA and 7 regions of interaction (10). The architecture of nucleosome, therefore, has a significant effect on accessibility of DNA for protein and molecular interactions. Despite this structural confinement, nucleosomal DNA has a high degree of freedom allowing it to accommodate binding interactions and adjusting to positioning signals (10). Nucleosomal DNA undergoes dynamic alteration with respect to the histone octamer to optimize the location of the positioning signals with respect to histones (10). This dynamic optimization and repositioning is likely to be dependent on the DNA sequence, with some sequences having higher or lower propensity to dynamically adjust with respect to the histone octamer (10). It is likely that this conformational flexibility is stronger or weaker depending on the DNA sequence and may facilitate the function and access of chromatin remodeling factors and other cellular regulatory factors (10). Thus, it is established that the interactions between the histones and the minor grooves are responsible for conformational flexibility and dynamic alterations of the nucleosomal DNA structure. In addition to bringing about the first level of DNA compaction and providing a scaffold for chromatin-related processes and binding of chromatin enzymes, the nucleosome has a third fundamental function—self-assembling into higher order chromatin structures to allow further compaction of the genome (11).

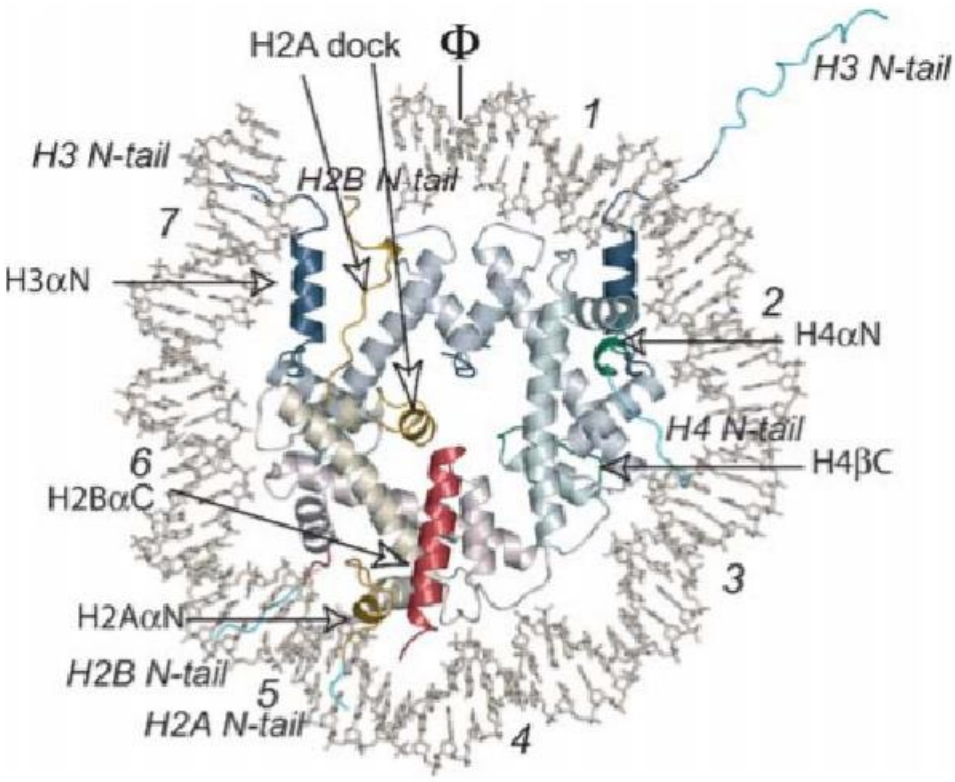

Figure 7: Overview of the nucleosome structure. Numbered regions 1 through 7 indicate regions of contact between the DNA minor grooves and the histone proteins *(10)*.

1.4. Chromatin Fiber

Nucleosomal array is the first level of DNA compaction in the nucleus. Higher order organizations and compactions are needed in order to fit the DNA inside the nucleus. The next level of structural organization of DNA is the compaction of nucleosomal array into chromatin fiber. This secondary structure is the first level of higher-order compaction which results in a 30 nm chromatin fiber (11). Very little is known about the morphology of the chromatin fiber and the mechanisms that fold and organize chromosomal arrays into three-dimensional fibers. Two models have been proposed for the structure of the chromatin fiber: the solenoid model and the

zigzag model (13). The solenoid model is an interdigitated one-start helix, while the zigzag model is a two-start helix with the linker DNA crisscrossing between adjacent rows of nucleosomes (14). The fiber itself exists in two forms. The first is the extended fiber observed at low ionic strength with a diameter of approximately 30 nm. The second form is the condensed or compact fiber with very similar diameter and an irregular, kinky conformation, with very rare regions of regularity (15). Chromatin fiber in its more condensed conformation is considered much less active than the extended conformation because the regions of interaction and binding sites are less accessible. The structural compaction of the chromatin fiber must be reversible. These fibers in their condensed form must be able to change to a more extended conformation to allow processes like transcription, replication, and repair (15). The structure of the chromatin fiber in condensed or extended form is very hard to visualize because it is too compact. The study of these fibers requires sophisticated biophysical and biochemical methods.

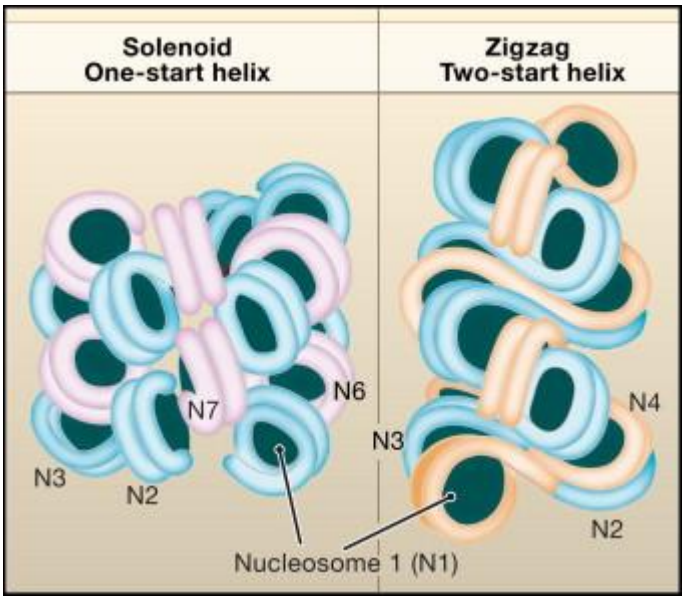

Figure 8: the solenoid and zigzag models for chromatin fiber *(13)*.

1.5. Chromosomal Structure

The chromatin fiber during cell division undergoes a massive 250-fold compaction organizing itself into a metaphase chromosome—the most condensed form of chromatin structure. This structure, however, just like other organizational orders of chromatin, is not inert. The condensation and decondensation of chromosomes regulated by reversible modification of chromosomal proteins lead to gross morphological changes in the chromatin structure during the cell cycle (4). Two principal models have been proposed for the architecture of the chromosome. The radial arrangement model suggest that the chromatin fiber organizes itself into loops. The second model proposes a helical folding (4). There is a third model that suggest a networked organization of the chromatin fiber (16). However, these models cannot be certainly verified or distinguished using conventional microscopy methods. The most studied model is the loop model. Considerable evidence from studies supports the organization of the 30 nm chromatin fiber into loops connected at an axis that constantly assembles and disassembles itself (4). These loops further organize into more complex structures that eventually form the chromosome. The hierarchical order is such that at the 30-nm fiber first folds into 100-130 nm chromonema fiber which folds into 200-250 nm prophase chromatid and further into 500-750 nm metaphase chromatid (16). Figure 9 illustrates these hierarchical folding of the chromatin fiber into metaphase chromatid.

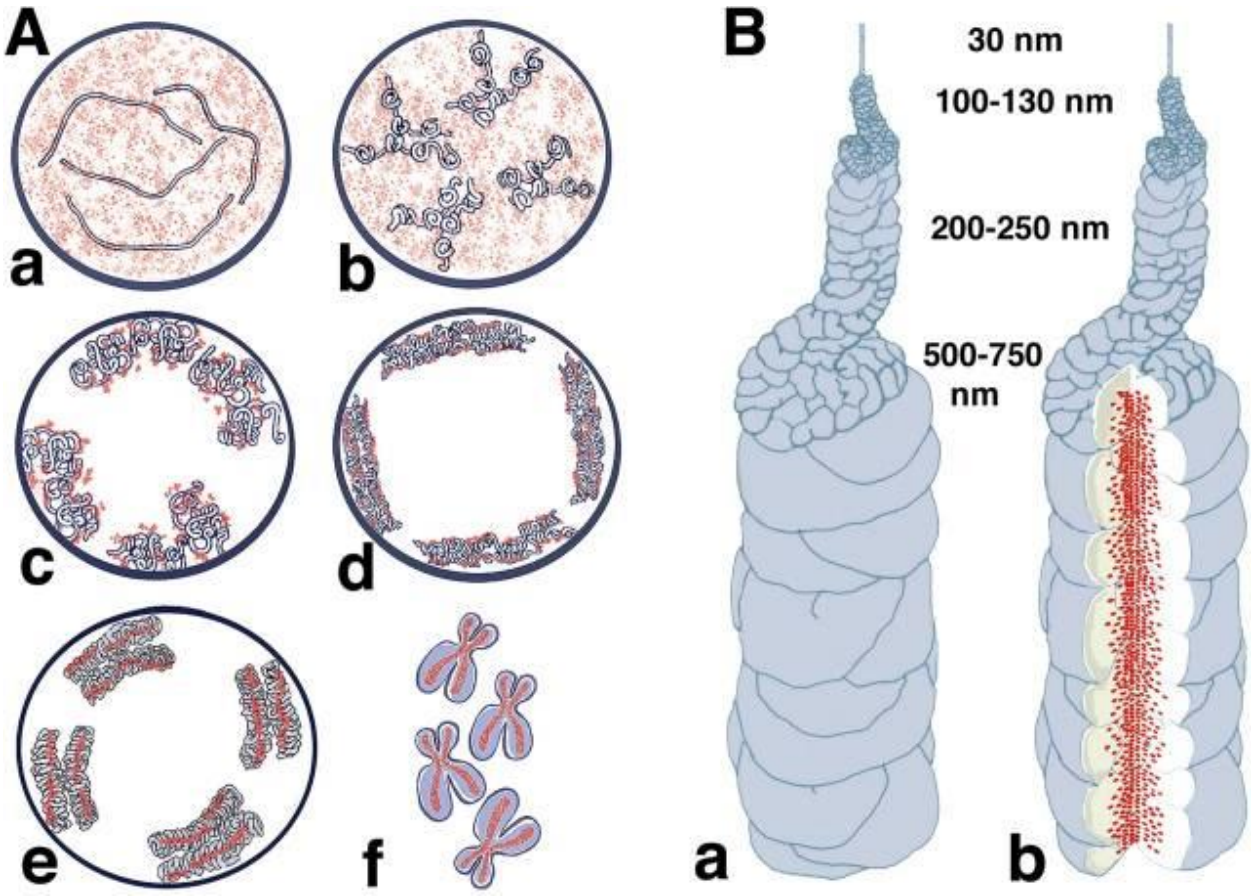

Figure 9: Axial model of the chromosome. Chromatin fiber through a hierarchical folding process organizes itself into metaphase chromosome *(16)*.

1.6. Chromatin Function

The fundamental and widely known function of chromatin is to condense the genetic material into compact packages that can fit inside the eukaryotic nucleus. This primary function of chromatin structure, however, controls, affects and regulates many other cellular functions in the nucleus. Chromatin structure plays an important role in DNA damage response by undergoing dramatic reconfiguration to facilitate access of DNA repair factors (17). Failure of the local chromatin configuration to enable DNA damage response may be the cause of many epigenetic diseases and disorders. Moreover, chromatin regulates other functions such as

DNA methylation, replication, recombination, and repair (18). There are other vital functions in which chromatin structure plays a crucial role. One such process is the cell division. Chromatin undergoes dramatic reconfiguration and remodeling as the cell transitions between the different phases of the cell cycle facilitating the division and transfer of the genetic material to the two daughter cells (19). The implications of this function are far reaching as they determine the proper formation of fully functioning, healthy cells. Understanding the remodeling and re-organization of the chromatin structure during cell division can shed light on many disease mechanisms. However, despite advances in microscopy techniques, the structure of chromosomal chromatin is still one of the major challenges in structural biology. In addition to that, emerging evidence suggest that the mechanical properties of the nucleus such as stiffness and deformability are a deciding factor in facilitating the spread of tumor cells from the primary tumor to distant organs causing cancer metastasis (20). Since chromatin is one of the primary contents of the nucleus, the stiffness of the chromatin structure can play an elemental role in nuclear deformability and mechanobiology of the cell. In this paper, chromatin structure and its conformational characteristics during cell division as well as chromatin's mechanical properties in metastatic tumor cells are the subject of thorough investigation.

Chapter Two: Background

2.1 Mitotic Cell Division and Chromatin Compaction

Mitosis is a cell division process by which the genetic material is duplicated and separated resulting in the formation of two identical daughter cells. Mitosis is the fundamental mechanism for proliferation, growth, and repair in eukaryotic cells. There are five stages of mitosis: prophase, prometaphase, metaphase, anaphase, and telophase. The hallmark of prophase is the onset of chromosome condensation. Prophase is the stage when replicated chromosomes condense and compact to form sister chromatids, joined at the central point called centromere (22). Two protein complexes, condensin I and condensin II, regulate the condensation of mitotic chromosome. These proteins encircle DNA and disassemble interphase chromatin to facilitate formation of mitotic chromosomes (23). During prometaphase, the nuclear envelope breaks down mixing the nuclear material with the cytoplasm. In metaphase, the stage that will be studied and compared with interphase in this paper, condensed sister chromatids are aligned in the equatorial plane along the center of the cell. During anaphase, sister chromatids are separated at their centromere and pulled to the opposite poles of the cell. It is essential that during anaphase each daughter cell is provided with an identical set of chromosomes. The final stage of mitosis is telophase during which each set of chromosomes is wrapped in a nuclear membrane separating the nuclear DNA from cytoplasm. Following the formation of nuclear envelope, a separate process called cytokinesis takes place which divides the parental cytoplasm into two separate daughter cells (22). Figure *10* depicts the schematic of all the five phases of the cell cycle as well as cytokinesis.

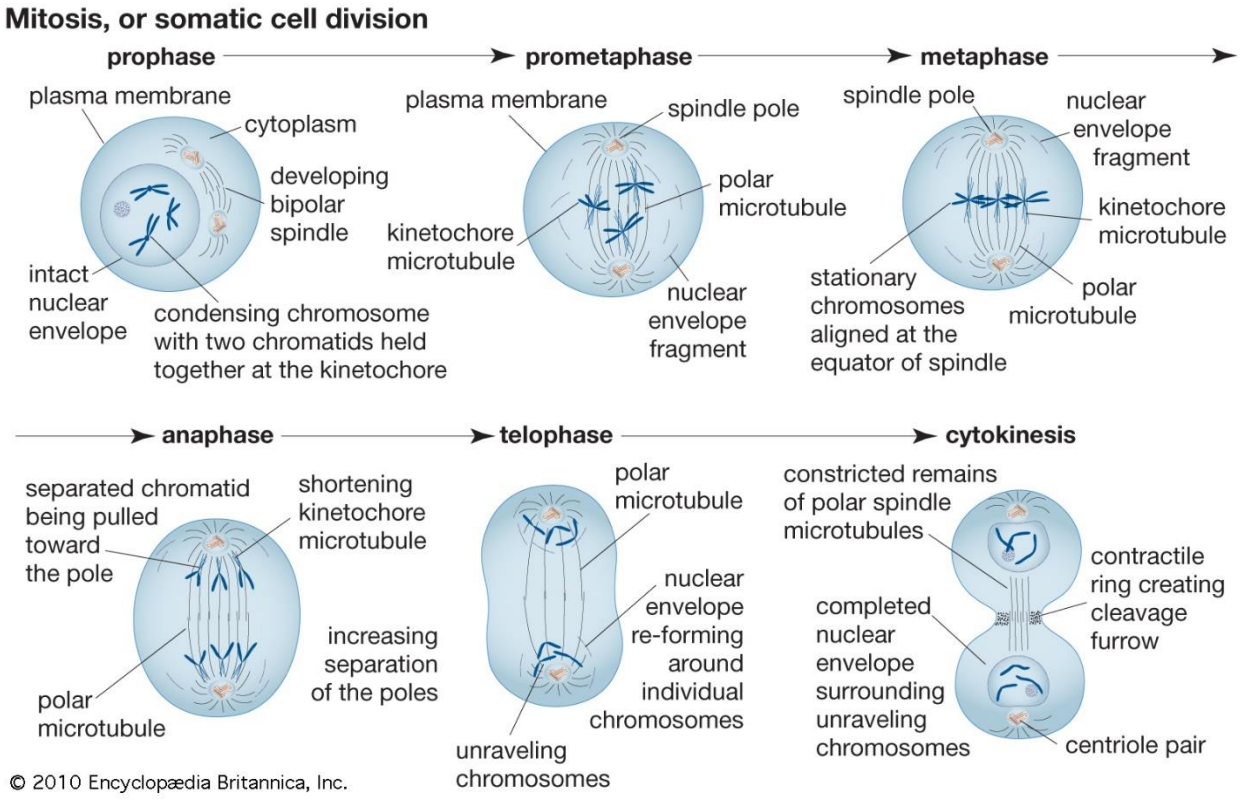

Figure 10: Stages of mitotic cell division. During metaphase, chromosomes are at the most condensed state *(24)*.

Mitotic chromosome structure must fulfil three major tasks to ensure proper chromosome segregation and formation of two fully functioning identical daughter cells (25). If any of these tasks is not fully and perfectly performed, it will have consequential effect on the fate of the cell which can disrupt many cellular functions and even lead to many diseases. The first and most important task of mitotic chromosome is proper compaction of the genetic material to ensure that the cell division process can take place inside the small nuclear space. The second task of the chromosome is to develop the required mechanical properties such as rigidity and bendiness to enable drastic movements of the genetic material during mitosis. And finally, the structure is responsible for proper partitioning of chromosomes by creating topological barriers between the

two sister DNA molecules as well as each individual chromosome –a task called chromosome individualization (25).

The structure of mitotic chromosome is still a big mystery in biology. The chromosome reaches its most compact state as it proceeds from interphase to metaphase. However, this organization to these higher-order structures and its mechanism is a subject of debate. Two structural states have been attributed to chromatin: heterochromatin and euchromatin (19). Heterochromatin is the more compact fraction of chromatin and remains condensed throughout the cell cycle except for DNA replication stage. It is replicated late in the S-phase, has low gene density, and is believed to be inactive in transcription. This state is associated with pericentromeric and telomeric regions of the chromosome. This facultative heterochromatin interconverts between heterochromatin and euchromatin in response to several factors such as methylation and acetylation. The euchromatin, on the other hand, is the chromatin fraction that contains genes and is active in transcription. Euchromatin is replicated early in S-phase and is relatively decompacted and decondenses during interphase (19). Figure 11 depicts the formation of heterochromatin and euchromatin as a result of DNA methylation and acetylation causing the nucleosomes to pack together tightly and loosely respectively. Chromatin compaction and structure during mitotic cell division is especially important as it can influence the fate of the resulting daughter cells. In this research, chromatin compaction in metaphase chromosomal structure is the subject of thorough investigation using Fluorescence Lifetime Imaging and phasor analysis.

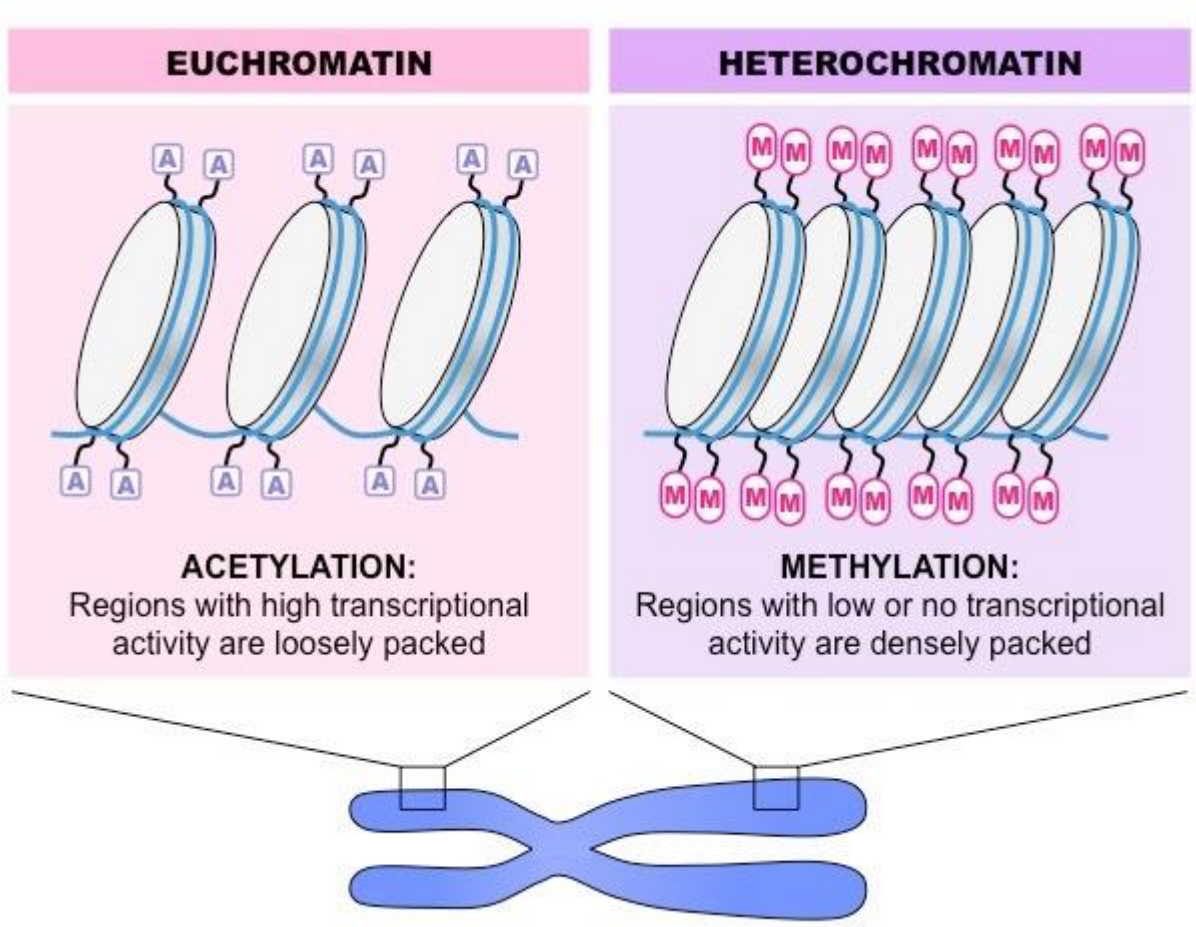

Figure 11: Heterochromatin substructure is densely packed and is formed in response to methylation. Euchromatin is loosely packed and is formed as a result of histone acetylation *(26)*.

2.2 Nuclear Deformability and Cancer Metastasis

Metastasis is a process by which cancer cells break away from where they first started and spread through the body. The newly formed tumors in other parts of the body are metastatic tumors and are the same as the primary tumor. Cancer cells spread to distant parts of the body by travelling through the blood or lymph system (27). This process follows a series of steps. First the cells grow into and invade nearby tissues. From normal tissues they squeeze through the pores of the tissue and the walls of nearby blood vessels or lymph nodes. Moving through the

lymphatic system and bloodstream, these cells stop in small vessels and once again squeeze through the walls of the vessel and invade surrounding tissues. In the new tissue, cancer cells grow and form a metastatic tumor (27). Cancer metastasis is the primary cause of cancer morbidity and mortality. An estimate of about 90% of cancer-related deaths are caused by metastatic cancers (28).

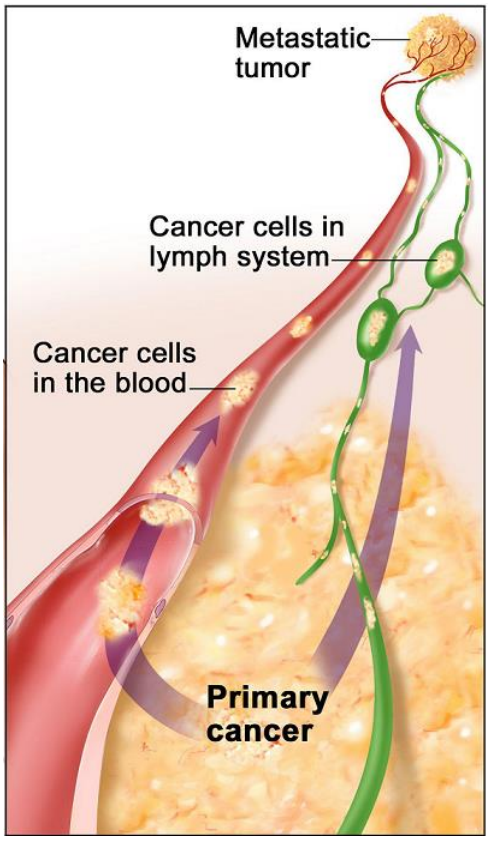

Figure 12: Cancer cells in the primary cancer travelling in the lymphatic system and bloodstream to a distant part of the body forming metastatic tumor *(27)*.

During the process of migration, cancer cells must pass through very small interstitial spaces that are much smaller in cross-section than the cell itself. These pores through which cancer cells squeeze are on the order of 0.1 to 20 µm in diameter (21). As a result of migrating through such confined environments, these cells experience considerable mechanical stress.

Since the largest and stiffest organelle in the cell is the nucleus, it undergoes frequent and severe nuclear deformation and nuclear envelope rupture during migrations (21). Nuclear envelope regains it integrity quickly. However, the transient rupture causes uncontrolled exchange between the nucleoplasm and cytoplasm exposing DNA to cytoplasmic components and ultimately causing DNA damage. This acquired damage leads to genomic instability of these cancer cells and enhances their metastatic potential and resistance to therapies (21). Therefore, the deformability of the nucleus is emerging as an important factor facilitating mechanisms by which cancer cells metastasize. Since chromatin is a major constituent of the nucleus in the cell, there could be positive correlation and even causation between chromatin and nuclear stiffness and deformability.

In this research, Fluorescence Lifetime Imaging, and phasor analysis of the lifetime of a nuclear probe are used to investigate and report on stiffness and deformability of chromatin. Three different cell lines are studied. The MCF10A cell line is used as control. These cells are non-malignant breast epithelial cells and commonly used as a model to study normal breast cell functions and transformation (29). Since these cells do not metastasize, they are a suitable control model to examine their cellular mechanobiology compared with that of aggressive metastatic tumor cells. The second cell line in this study is the MCF7 cells. A human breast carcinoma line, these cells, even though not the most aggressive cancer type, metastasize to lungs, liver, and spleen (30). The third cell line is MDA-MB-231. These cells are highly aggressive and invasive triple-negative breast cancer (TNBC) cells. Triple-negative cancer cells have very limited treatment options. The MDA-MB-231 cells preferentially metastasize to the bones, brain, and lungs (31). The objective of this research is to examine and compare softness or stiffness and deformability or rigidity of chromatin in these three cell lines. The MCF10A cell

line is expected to show higher mechanical stiffness and rigidity, while the MB-231 cell line is expected to have the softest and most deformable properties. And finally, the MCF7 cell line is expected to be softer than MCF10A cells but not as deformable as MB-231 cells.

Chapter Three: Methods and Materials

3.1 Fluorescence Lifetime Imaging (FLIM)

Fluorescence Lifetime Imaging Microscopy (FLIM) is a powerful biomedical imaging technique that detects and measures dynamic changes in microenvironmental parameters of fluorophores as well as kinetic interactions and conformational changes in the molecular environment. Due to its high sensitivity to microenvironmental changes, FLIM is capable of monitoring changes in parameters such as temperature, viscosity, pH, and ion concentration (32). This technique is more robust than intensity-based imaging because the fluorescent lifetime does not depend on concentration, absorption by the sample, sample thickness, photobleaching and excitation intensity (32). The fluorescence lifetime, on the other hand, depends on a wealth of environmental parameters as well as molecular proximity and binding. Therefore, FLIM is the technique of choice for many functional imaging applications. (33). There are two approaches to implementing FLIM. It can be done in frequency domain or in time domain and involves modulating or pulsing the exciting light (34). FLIM produces images that are based on the excited state decay rate of fluorophores. That is the time it takes for an excited molecule to decay back to the ground state. This decay rate is called the fluorescence lifetime and is defined as the average time that a molecule remains in an excited state before emitting a photon to return back to the ground state (33).

Fluorescence process and its lifetime can be explained by the principles of the Perrin-Jablonski diagram. A molecule can be excited from the ground state into higher singlet electronic states. From there, it can undergo rapid thermalization processes to decay to the first singlet electronic state. These radiationless processes which take place on the order femtoseconds

include vibrational relaxation and internal conversion (34). Once in the lowest vibrational level of the first singlet excited electronic state, the molecule can decay back to the ground state by emitting a photon. This decay process by the means of detectable photons is called fluorescence which occurs on the order of nanoseconds (32). Since the excited molecule undergoes thermal processes that reduce its energy to a lower level before emitting a photon, the emission occurs at a longer wavelength than the excitation. This shift in emission wavelength is called the Stokes shift, after George Stokes who first observed this phenomenon (34). Another characteristic of the fluorescence process is that the emission spectrum for any molecule remains the same regardless of the excitation wavelength. This is because fluorescence always occurs when a molecule decays from the lowest vibrational level of the first singlet electronic excited state (S_1) to the ground state (S_0) (32). The molecule can decay back to the ground state without emitting a photon, in which case the process is a non-radiative decay. If the excited molecule undergoes intersystem crossing and decays to the ground state from an excited triplet state, the process is called phosphorescence. Phosphorescence is a much longer process and occurs on the order of milliseconds to hundreds of seconds (32). The Jablonski diagram depicting the excitation and decay processes is shown in Figure *13*.

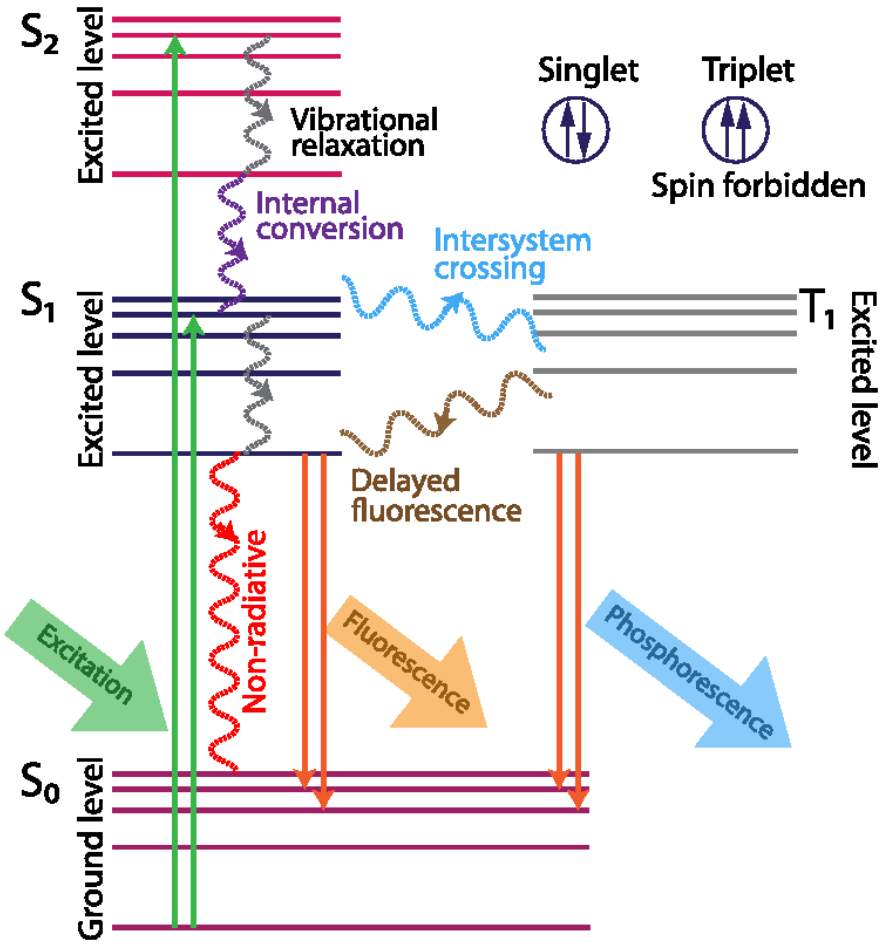

Figure 13: Schematic of the Jablonski diagram illustrating excitation from and decay to the ground state through different processes *(32)*.

In the time domain approach, the fluorescence lifetime (τ) is the time it takes for the intensity I(t) to decrease to 1/e or 36.8% of its original value. And the value of intensity as a function of time is a first-order kinetic equation for all species, i, in the environment (32). The equation for the decaying intensity is given in equation (1)

$$I(t) = \sum_i \alpha_i e^{-\frac{t}{\tau_i}} \qquad (1)$$

where α, the amplitude of the exponential function, is called the pre-exponential factor and indicates fractional contribution of each species. In a multiexponential sample, the average lifetime of the mixture is the sum of the lifetime of each species weighted by fractional contribution of each species (32). The equation for the mean lifetime is

$$\tau_m = \sum_i \tau_i \alpha_i \qquad (2)$$

As mentioned earlier, FLIM can be implemented in either time domain or frequency domain. Both approaches have their unique advantages and disadvantages depending on the specifics of the experiment and the kind of processes that are being studied. In the time-domain method, the fluorophore is excited by a short pulse of light and the decaying intensity of the emission versus time is recorded (34). The decay is then calculated using time-of-arrival of photons or other methods such as time-gated detection or pulse sampling (32). If the decay signal is a single exponential, which means there is only one species fluorescing, and the lifetime is much longer than the exciting light, the lifetime is simply determined from the slope of the intensity curve, as shown in Figure *14* (34). If the lifetime is short compared to the exciting light, sophisticated mathematical tools need to be utilized to deconvolve the excitation signal from the emission decay signal. Very fast laser pulses, however, are often much shorter than most lifetime values making deconvolution procedures not as important and necessary (34). If there are different lifetimes, due to having a mixture of fluorophores or subtle interactions of fluorophores with their environment, the decay signal will be a multi-exponential decay function, which is the case for most biological systems (34). In these scenarios, calculating the lifetime is more complex and mathematically involved than a single exponential decay lifetime. Figure *14* illustrates a single

and a two-exponential decay signal versus time. Figure *15* shows intensity images of an excited sample with a multiexponential lifetime at different timepoints within its lifetime.

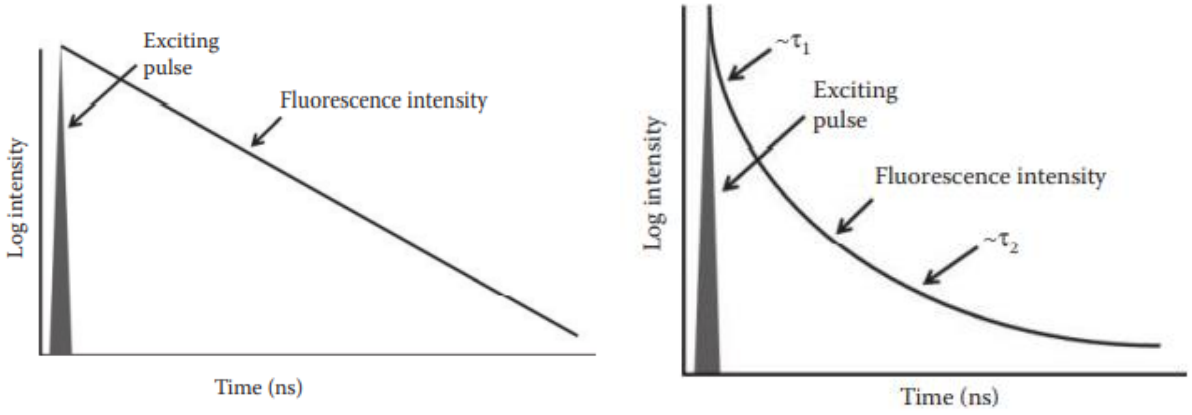

Figure 14: Intensity curve of a single and double-exponential decay signal *(34)*.

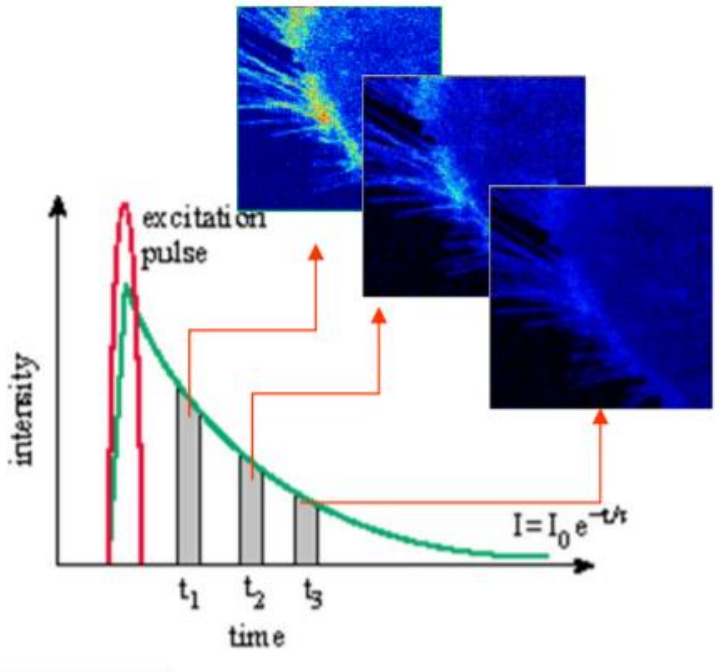

Figure 15: An excited sample at different time points within its lifetime *(39)*.

In the frequency-domain method, also known as harmonic method, the sample is illuminated by a continuous excitation light the intensity of which is sinusoidally modulated at high frequencies (32) (34). The equation for this excitation signal is

$$E(t) = E(0)[1 + M_E Sin(\omega t)], \quad (3)$$

where E(t) is intensity at time t and E(0) is the initial intensity at t = 0. The excitation modulation factor M_E is how much the amplitude of the sinusoid wave is modulated. The angular frequency equals $\omega = 2\pi f$, where f is the linear modulation frequency. Therefore, the emission signal is a sinusoidally modulated wave which is phase-shifted with respect to the excitation wave. This phase shift represents the delay between the absorption and emission of photons (32). The fluorescence signal emitted is written as

$$F(t) = F(0)[1 + M_F \sin(\omega t + \varphi)], \quad (4)$$

where F(t) is intensity of the fluorescence emission signal, F(0) is the initial intensity, M_F is modulation factor of the emission wave, and φ is the delay or phase shift between excitation and emission (32). The modulation factor for both excitation and emission signals is the ratio of AC to DC component of each respective wave signal. Therefore, the relative modulation is estimated to be

$$M_E = \frac{AC_{EX}}{DC_{EX}} \qquad M_F = \frac{AC_{EM}}{DC_{EM}} \qquad => M = \frac{\frac{AC_{EX}}{DC_{EX}}}{\frac{AC_{EM}}{DC_{EM}}}. \quad (5)$$

From relative modulation, the modulation lifetime τ_M is written as

$$M = \frac{1}{\sqrt{1 + (\omega\tau_M)^2}} \quad (6)$$

and the phase lifetime is written as

$$\tan \varphi = \omega \tau_{\varphi}. \quad (7)$$

In this method, lifetime τ can be calculated using the frequency and either the modulation or the phase shift, called modulation lifetime τ_M and phase lifetime τ_{φ}, respectively. If the decay is a single exponential, then these two lifetime values are equal. If the decay is a multiexponential, however, the phase lifetime is smaller than the modulation lifetime ($\tau_{\varphi} < \tau_M$) and both values depend on the modulation frequency (32) (34). For maximum sensitivity, the modulation frequency should be approximately the inverse of the lifetime (i.e., $\omega\tau = 1$) (32).

Acquisition speed is a major advantage of the frequency-domain technique over the time-domain technique making it the method of choice for imaging fast cellular processes. Data acquisition instrµments and electronic hardware also are important in improving temporal and spatial resolution as well as enhancing acquisition quality. An overview of the instrµmentation and devices is sµmmarized in the next section. Frequncy-domain FLIM is the method used in this research to study conformational changes of chormain during the cell cycle as well as chormatin's mechanical properties such as stiffness and deformability in cancer cells.

3.2 Data Acquisition and Data Processing Instruments

FLIM measurements in this study are taken using two-photon excitation laser scanning microscopy. Two-Photon Excitation (TPE) is a non-linear optical technique in which the energy of two photons absorbed simultaneously are combined. In this method, high-power, short-width pulses of laser are focused into the sample providing high photon density in a focused area eliminating the need for a pinhole (35). The wavelength of the resulting combined two photons is half, and its energy is twice that of each single photon. Therefore, the wavelength of the

excitation pulse should be set such that the combined energy of two photons is equal or greater than the energy band between the ground state and first electronic excited state of the fluorophore under study. A major advantage of TPE is that the longer wavelength of the excitation pulse is scattered much less inside the sample allowing for deeper penetration on the order of millimeters into the sample (35). And since the energy of the exciting pulse is lower, photobleaching and phototoxicity are reduced maximizing the probability of detecting an emission signal (36). Moreover, laser scanning microscopes (LSM) scan the sample point by point and block out-of-focus light producing higher contrast and spatial resolution compared to wide-filed microscopes (32).

Zeiss LSM880 with AiryScan is the system used for data acquisition. The sample is held in the incubation chamber at 37°C with 5% CO2. The fluorophore is excited with a Ti: Sapphire pulsed laser at 80MHz frequency with a wavelength of 800nm. The FLIM data is acquired using the Fast FLIM system which is controlled by SimFCS. SimFCS is a proprietary software created and licensed by the Laboratory for Fluorescence Dynamics (LFD). It is used to establish and control computer-hardware interface and for post-processing of collected data. The pixel dwell time is set to 16.38 µs and the frame size is 256x256 pixels. To increase signal to noise ratio, at least 100,000 photons are collected per each dataset. To achieve this number, 40 frames are taken for each FLIM measurement. The emission photons are collected at channel 1 through a 460/80 nm NADH filter. This filter is chosen to optimize signal detection based on the excitation/emission characteristic of the nuclear probe that is used in this study. Section 3.4 provides a brief description of the characteristics of the probe used in this research.

3.3 Analysis Method: Phasor Analysis

The phasor approach to fluorescence lifetime imaging is a powerful tool for data visualization and analysis. It is a fit-free method that provides spatial information and precise quantitative analysis about mixtures of fluorophores, Forster resonant energy transfer (FRET) and autofluorescence (37). In this method the decay signal at each pixel is transformed into a point representing modulation and phase of the signal providing a global view of the fluorescence process at each pixel (38). In this graphical global view, pixels with similar lifetimes are clustered together providing a visual distribution of the fluorophore species in the image (32). At each pixel, the histogram of the time delay, namely the values of sine-cosine signals, is transformed into the phasor space represented in a polar coordinate system plotting a two-dimensional histogram (38). For frequency-domain measurements, the values for these two coordinates, g(ω) and s(ω), at each pixel (i,j) are calculated using the following equations:

$$g_{i,j}(\omega) = M_{i,j}\cos(\varphi_{i,j}), \tag{8}$$

$$s_{i,j}(\omega) = M_{i,j}\sin(\varphi_{i,j}), \tag{9}$$

where $M_{i,j}$ is the modulation and $\varphi_{i,j}$ is the phase shift of the emission signal at pixel (i,j). The phasor coordinates are related to the lifetime τ and angular frequency of the laser pulse ω. For a single exponential decay these relationships are:

$$g_{i,j}(\omega) = \frac{1}{1 + (\omega\tau)^2}, \tag{10}$$

$$s_{i,j}(\omega) = \frac{\omega\tau}{1 + (\omega\tau)^2}. \tag{11}$$

Therefore, all single exponential decays fall on a semicircle of radius 0.5 centered at (0.5, 0). This circle is called the universal circle (38). The shorter the lifetime, the closer is the point on the universal circle to (1,0), which corresponds to $\tau = 0$, and the longer the lifetime, the closer the point is to (0,0), which corresponds to $\tau = \infty$, on the phasor plot (32) (37). Phasors have linear properties. This means a heterogeneous sample with two species has a phasor distribution that is on a linear line connecting the lifetime location of the two individual species on the universal circle (32) (37). Likewise, a three-exponential decay falls inside a triangle formed by three individual phasor locations (32). Figure *16* illustrates schematics of the phasor plot and the Universal Circle, and the location of single and double-exponential samples. Figure *17* shows individual phasor plots of fluorescein and Rhodamine B1 located on the Universal Circle along with a sample of their mixture located on the line connecting the two individual phasor positions.

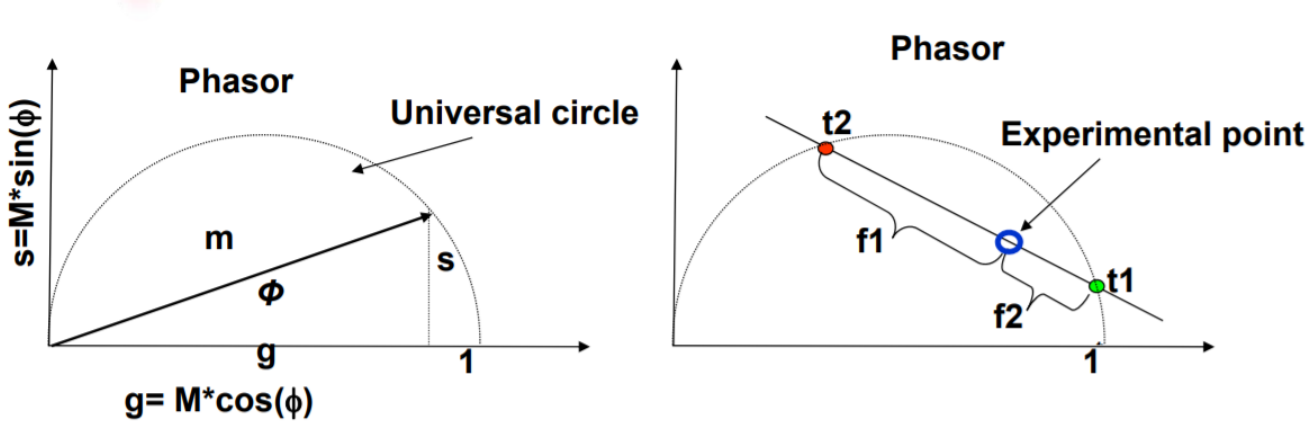

Figure 16: Phasor coordinates and the Universal Circle (left). Single and multi-exponential decays on and inside the Universal Circle (right) *(39)*.

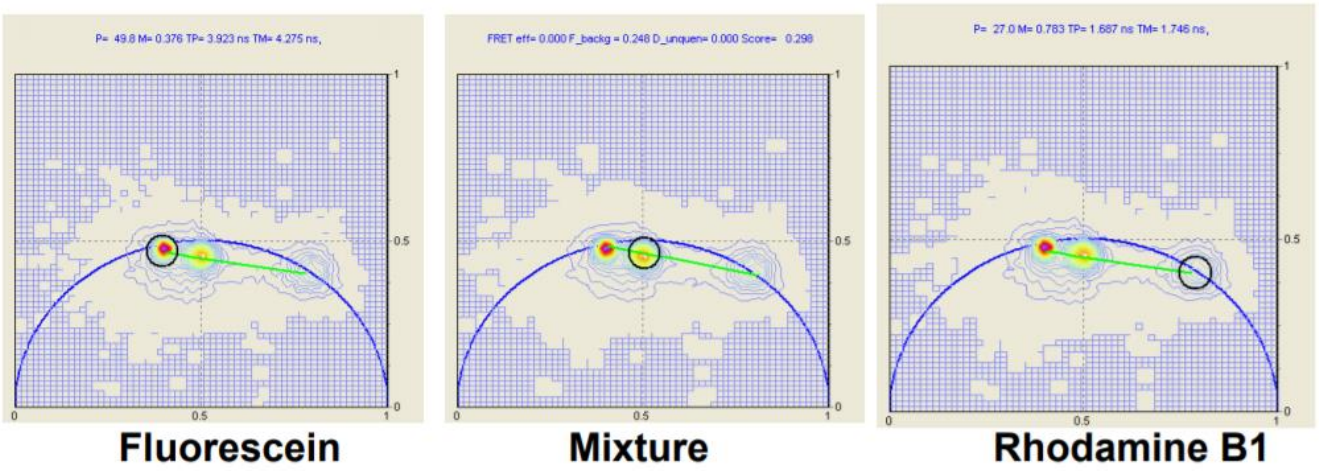

Figure 17: Phasor plot of two individual single-exponential fluorophores (Fluorescein and Rhodamine B1) and a sample of their mixture plotted in SimFCS *(39)*.

3.4 Nuclear Probe: Hoechst 33342

Hoechst 33342 Ready Flow Reagent cell permeable DNA stain is used to label chromatin. It binds DNA minor grooves and when bound has a quantum yield of 0.92 (19). It is excited by UV light at around 361 nm and emits blue fluorescence with an emission maximum of 461 nm. The sample is incubated with different concentrations of Hoechst for at least 30 minutes before FLIM data is acquired. The lifetime of Hoechst and changes to the lifetime with respect to concentration are quantitatively analyzed to gain information about conformational (size and accessibility) and mechanical properties (stiffness and deformability) of chromatin under different conditions.

Chapter Four: Interphase and Metaphase Chromatin

Metaphase and interphase Hela cells were labeled with Hoechst 33342 nuclear staining dye and were imaged at different concentrations of the probe. The objective of this experiment was to observe the binding behavior of the probe and explain it in terms of size, softness, and accessibility of chromatin structure during interphase and metaphase. Imaging and FLIM measurements were done in interphase and metaphase Hela cells. The cells were labeled with different concentrations of Hoechst 3342. Six different concentrations were imaged and measured: 0.05 µmol, 0.2 µmol, 0.4 µmol, 1.0 µmol, 2.0 µmol and 3.0 µmol. The binding mechanism of the probe to the binding sites was examined to see if the binding behavior followed aproximately the same pattern in all cells or was cell specific and different for each indivual cell. For that purpose, two approachs for labeling and measurement were adopted. In the first group, imaging and FLIM measurements were done on the same cells while the concentration was increased from 0.05 µmol to 3.0 µmol. In the second group, the cells under measrement were not kept constant. In this approach the effect of cell variation on lifetime measurements was investigated. The results showed that in general the binding behavior was independent of the cell under investigation and was approximately the same in all cells.

Next the binding behavior of Hoechst 33342 in metaphse and interphase Hela cells was investigated. Metaphase and interphase cells at the same 6 concentrations of Hoechst were imaged and their respecitve lifetime measurements were collected. The objective of this part of the experiment was to deduce information about the size, softness and accessibility of the binding regions in metaphase and interphase chromatin. Consequently, information about chromatin conformation, compaction, and accessibility in metaphase and interphase would be inferred, and chromatin structure in these two phases of the cell cycle would be comparetively

studied. Figure *18* shows metaphse and interphase chromatin at all 6 concentrations of Hoechst 33342. There is an obvious reduction in intensity in interphase chromatin starting at 1 µmol of Hoechst, and the quenching contunues to increase as the concentration of the probe in the environment is increased.

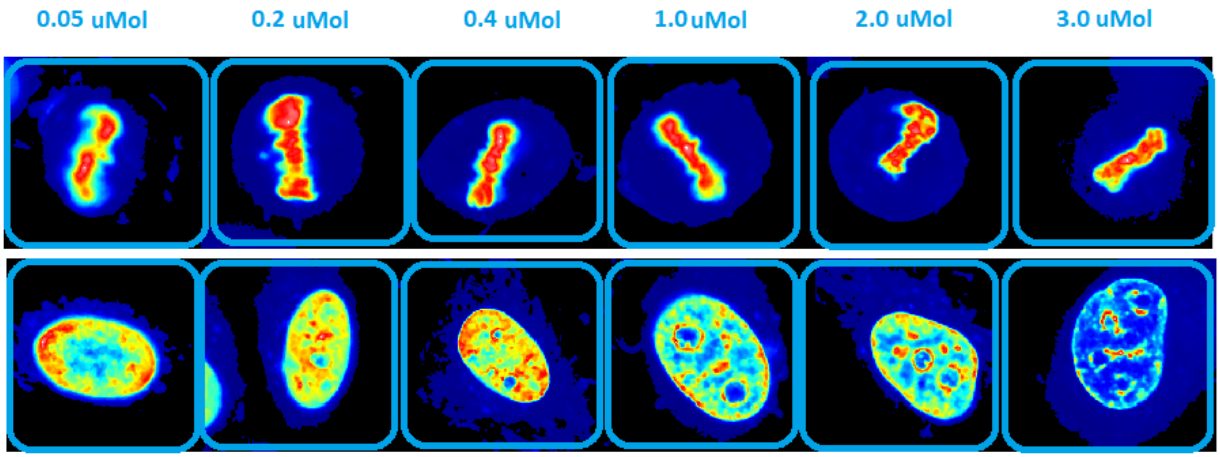

Figure 18: Metaphase (top row) and Interphase (bottom row) chromatin labeled with different concentrations of Hoechst 33342 (starting from 0.05 micro-mol to 3 micro-mol)

4.1 Results

4.1.1 Interphase Chromatin

In total, 63 interphase Hela cells were imaged. Of those, 5 cells were labeled with 5 micro-mol of Hoechst 33342, 5 cells with 0.2 µmol, 18 cells with 0.4 µmol, 13 cells with 1 µmol, 14 cells with 2 µmol and 8 cells with 3 µmol. The imaging and measurements were done at laser frequency of 80MHz. For each cell, values for intensity, G and S coordinates, modulation lifetime (tau lifetime) and phase lifetime (tau phase) were calculated at every pixel. Contours of the phasor coordinates as well as trajectory of the phasor were calculated and plotted pixel by pixel as shown in Figure 19. The linear trajectory depicted using pseudo-color gradient shows a shift towards shorter lifetime at higher concentrations of the probe. Green pixels represent longer lifetime and as the color is shifted toward red, the lifetime is decreased.

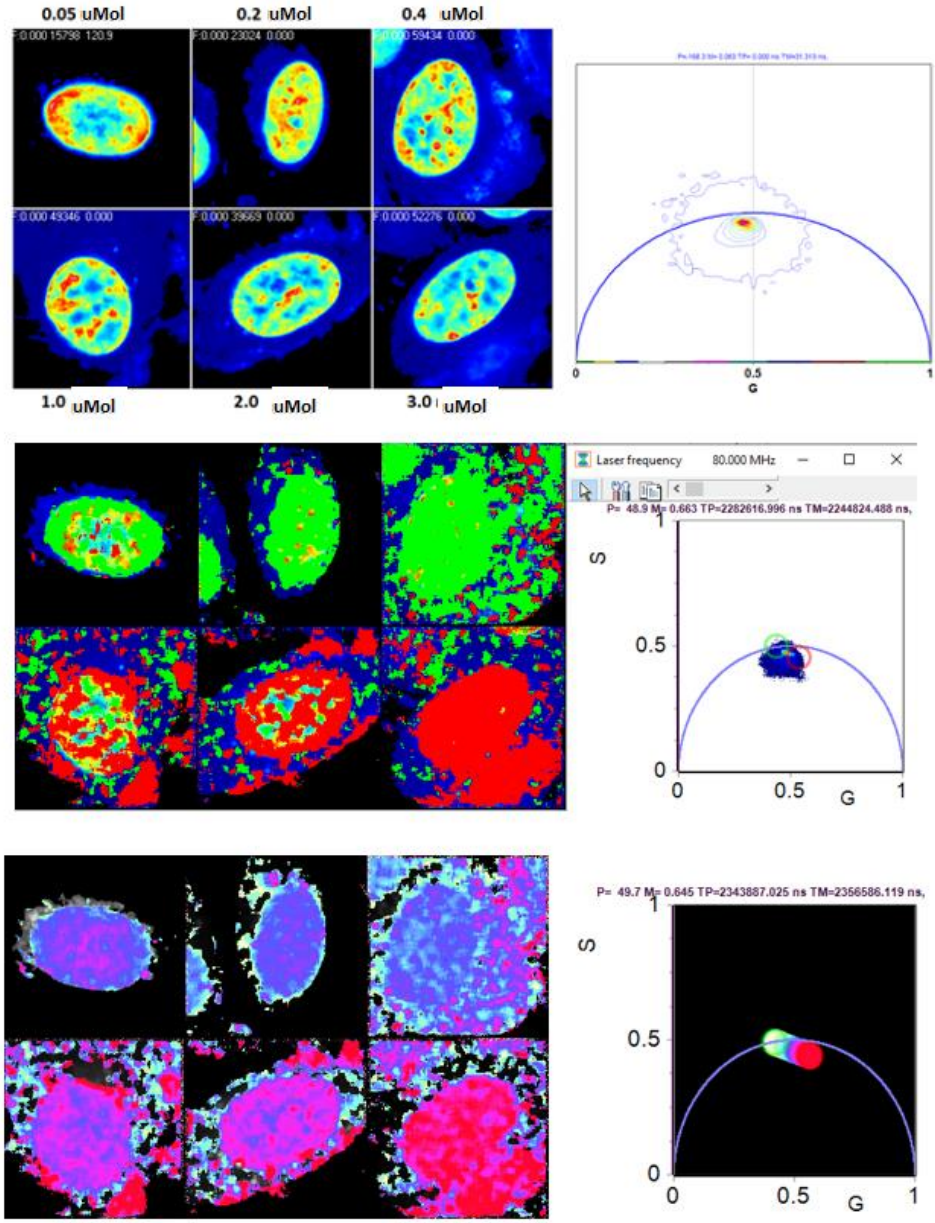

Figure 19:Phasor plot contour and trajectory for all concentrations of the probe.

For each cell, average values of intensity, phasor coordinates (G , S), tau lifetime and tau phase were calculated. The phasor plot in Figure 21 shows the average G and S values for each cell at each concentration. The phasor is shifted to the left (longer lifetime) as the concentration of the probe is increased from 0.0t to 0.2 and to 0.4 µmol of Hoechst 33342. However, as the concentration increased from 0.4 to 1 µmol, there is a sudden shift to the right (shorter lifetime)

in the phasor plot. At this point, the trend of the trajectory of the phasor is reversed and contunies to move toward shorter lieftime as more porbe is added, going from 1 µmol to 2 µmol and to 3 µmol. These results suggest that the binding model is different for the first three concentration groups than the last three concentration groups. Whether these differences in lifetime values are significant is the subject of further investigation in the next step of analysis. However, one possible explanation for these shifts in the phasor position is that at 0.05 µmol to 0.4 µmol the probe is binding to minor grooves that are more rigid and/or larger in size. As the concentration is increased from 0.4 µmol to 1 µmol, there is a sudden shift of the phasor toward shorter lifetime. Quenching could be the reason for that shift. However, further examination of intensity values, presented in Figure 20, shows that there is no quenching happening between 0.4 µmol to 1 µmol because the intensity slightly increases.

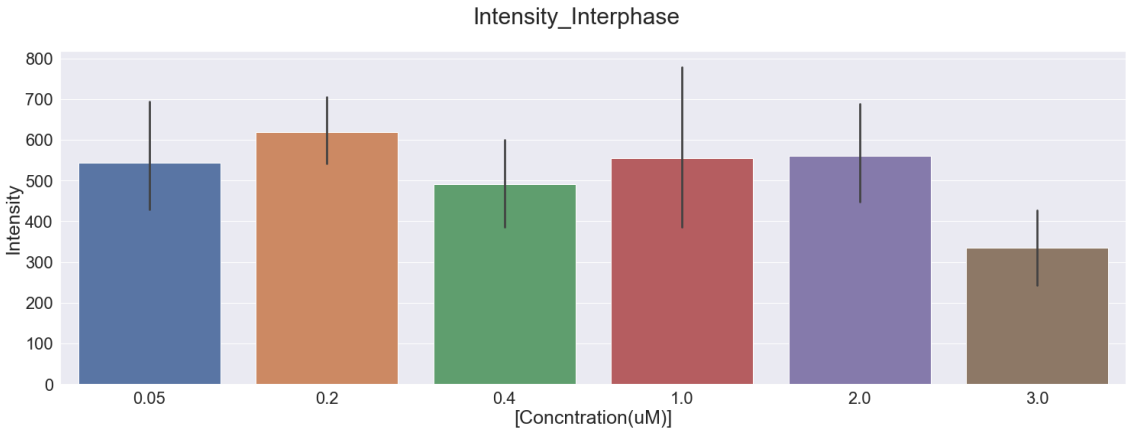

Figure 20: Average intensity values at each concentration.

Another more probable reason explaining the shift in the phasor could be that at 1 µmol, the probe begins binding to more softer regions of the chromatin or to minor grooves that are larger in size. This change of binding behavior could be happening because the more rigid regions are saturated and do not have any binding sites available. Another hypothesis could be

that a conformational change in the chromatin has made those rigid regions inaccessible and the more softer regions accessible to the probe.

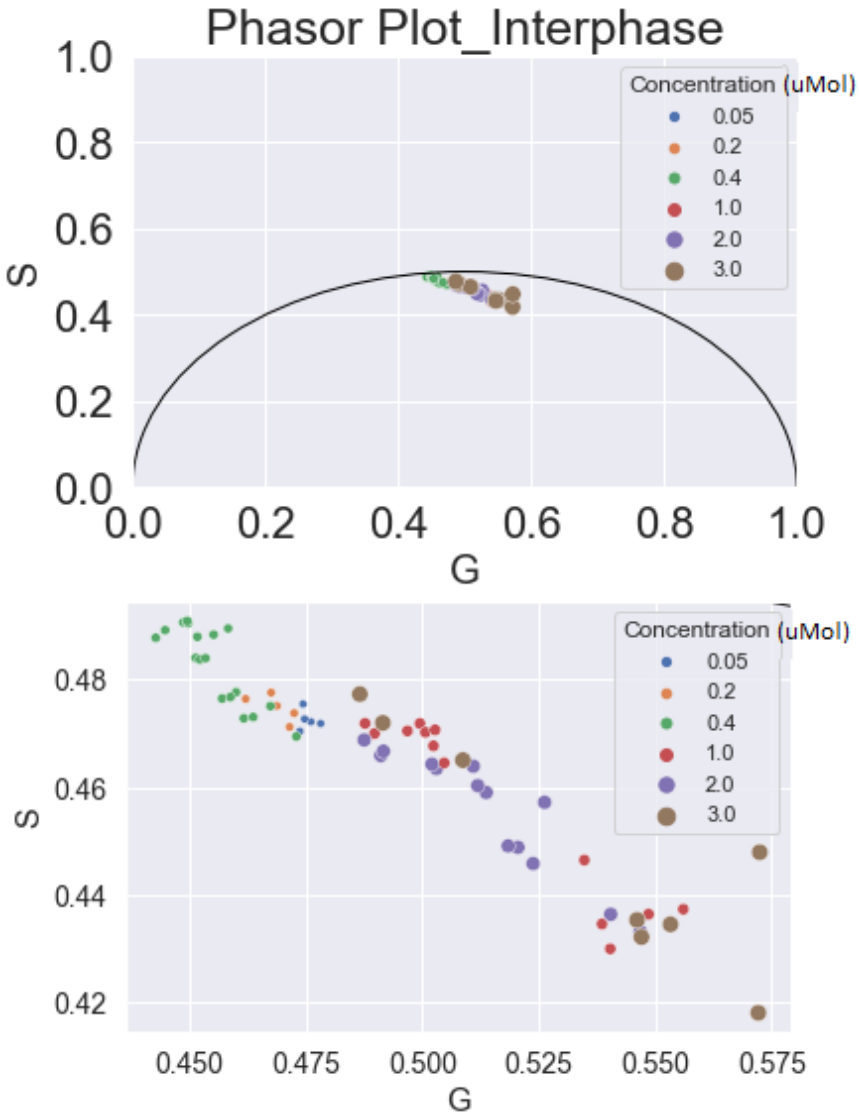

Figure 21: Phasor plot of Interphase chromatin showing the lifetime of Hoechst 33342 increasing almost linearly as the concentration increases

A closer look at the phasor plot reveals that there are two distinct clusters suggesting 2 different binding models which can be described and distinguished by different size, softness, and accessibility of the binding regions. The first cluster, shown in Figure 22, illustrates the increasing lifetime as the concentration of the probe is increased 8-fold from 0.5µmol to

0.4µmol. The second cluster shows the decreasing lifetime as the concentration is increased 3-fold from 1.0µmol to 3.0µmol. The spread of the second cluster for a 3-fold increase in the probe concentration seems to be more than twice as large as the spread of the first with an 8-fold increase in the concentration of the probe. To confirm these findings quantitatively, statistical analysis is performed on the phase and modulation lifetimes at all concentrations.

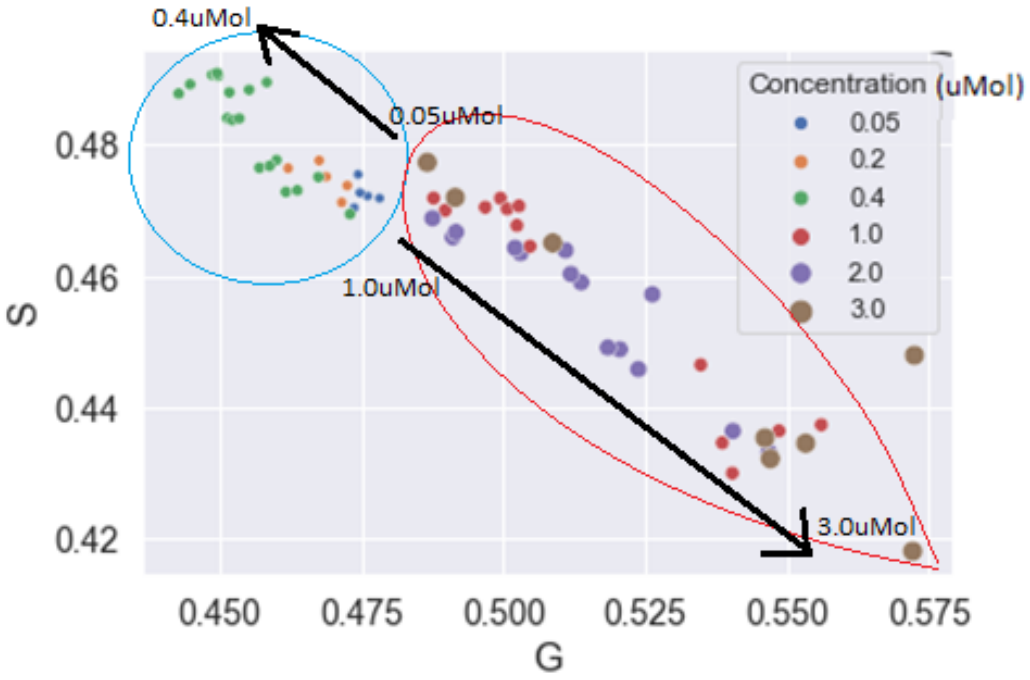

Figure 22: Two distinct clusters in the phasor suggesting two different binding behaviors for the probe.

The boxplot of tau modulation values, shown in Figure *23*, confirms the existence of two distinct clusters with different binding behaviors. The average value of modulation lifetime significantly increases from 2.20e-9 ±1.03e-11 to 2.24e-9±1.81e-11 seconds as the concentration is increased from 0.05µmol to 0.4µmol. The average lifetime for this cluster is 2.22e-9±1.37e-11 seconds. The second cluster has a significantly shorter modulation lifetime. In this cluster, however, there is no significant change in the lifetime as the concentration of the probe increases

from 1.0µmol to 3.0µmol. This second cluster has an average lifetime of 2.10e-9±6.41e-11 seconds among all three concentration, with a standard deviation that is almost 6 times larger than the first cluster. The result of statistical tests and the p_values signifying difference among groups is shown in Table 1.

Modulation Lifetime

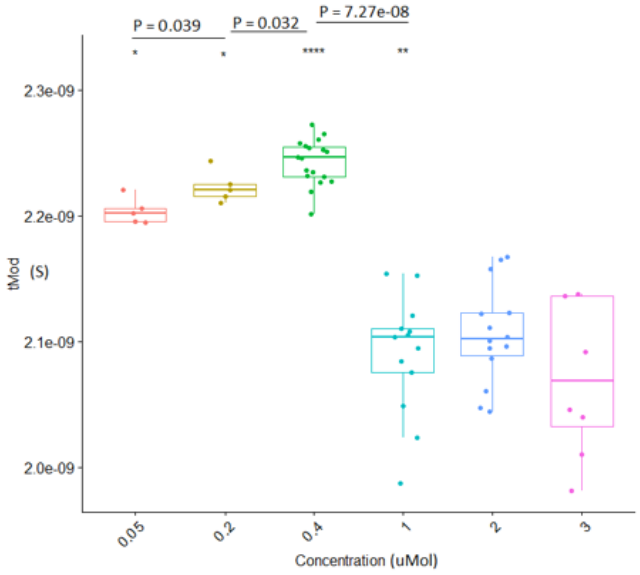

Concentration	N	Mean tau Mod	SD	SE	CI
0.05(uMol)	5	2.20E-09	1.03E-11	4.61E-12	1.28E-11
0.2(uMol)	5	2.22E-09	1.28E-11	5.74E-12	1.59E-11
0.4(uMol)	18	2.24E-09	1.81E-11	4.26E-12	8.99E-12
1(uMol)	13	2.09E-09	4.74E-11	1.32E-11	2.87E-11
2(uMol)	14	2.11E-09	3.96E-11	1.06E-11	2.29E-11
3(uMol)	8	2.10E-09	1.08E-10	3.83E-11	9.06E-11

Figure 23:: Boxplot of Tau Modulation values showing the mean value for each group and significant difference between the groups. The plot further confirms the existence of two distinct clusters of groups (0.05µmol to 0.4µmol increase in lifetime, and 1µmol to 3µmol has a significantly shorter lifetime with no significant changes between each group).

Table 1: significance test and p_values for modulation lifetime values of all 6 groups of concentrations. The diagonal shows consecutive groups. Modulation lifetime significantly changes as the concentration increases from 0.05µmol to 1µmol.The first cluster's binding model is associated with GC-rich minor grooves.

Concentration	0.05(µmol)	0.2(µmol)	0.4(µmol)	1(µmol)	2(µmol)
0.2(µmol)	3.97E-02	NA	NA	NA	NA
0.4(µmol)	1.53E-03	0.03209605	NA	NA	NA
1(µmol)	5.84E-04	0.000583567	7.27E-08	NA	NA
2(µmol)	5.84E-04	0.000583567	6.36E-08	5.23E-01	NA
3(µmol)	3.97E-02	0.03968254	3.15E-03	6.45E-01	3.81E-01

Phase Lifetime

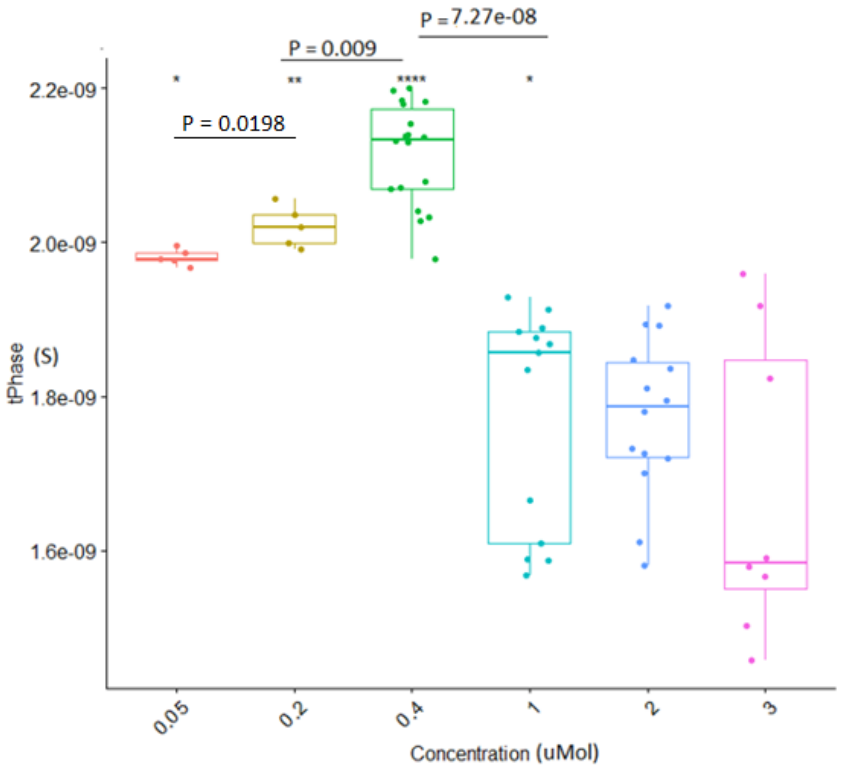

Concentration	N	Mean tau Phase	SD	SE	CI
0.05(uMol)	5	1.98E-09	1.09E-11	4.88E-12	1.36E-11
0.2(uMol)	5	2.02E-09	2.68E-11	1.20E-11	3.33E-11
0.4(uMol)	18	2.12E-09	6.66E-11	1.57E-11	3.31E-11
1(uMol)	13	1.77E-09	1.44E-10	4.00E-11	8.72E-11
2(uMol)	14	1.77E-09	1.02E-10	2.73E-11	5.90E-11
3(uMol)	8	1.67E-09	1.95E-10	6.91E-11	1.63E-10

Figure 24: Boxplot of phase lifetime values for all 6 groups.

The same patterns govern the chnages in the phase lifetime for all 6 groups, seen in Figure 24, further confirming that there are two models governing the binding behavior of the

probe as the concentration of the probe is increased. The average value of tau phase increses from 1.98e-9±1.09e-11 to 2.12e-9±6.66e-11 seconds. The phase lifetime seignificantly decreseas in the second cluster with higher concentration of the probe with average value of 1.77e-9±1.47e-10 for all three concentrations of 1µmol, 2µmol and 3µmol. There is no significant change between these three groups. Moreover, the standard deviation for the second cluster, 1µmol, 2µmol and 3µmol, is an order of magnitude larger than the first cluster. The result of statitical analysis comparing the phase lifetime values between each group is presented in Table 2.

Table 2: P_values for indicating statistical difference between Tau Phase at different concentrations of Hoechst 33342 in interphase chromatin.

Concentration	0.05(µmol)	0.2(µmol)	0.4(µmol)	1(µmol)	2(µmol)
0.2(µmol)	1.98E-02	NA	NA	NA	NA
0.4(µmol)	7.80E-04	9.16E-03	NA	NA	NA
1(µmol)	5.00E-04	5.00E-04	7.27E-08	NA	NA
2(µmol)	5.00E-04	5.00E-04	6.36E-08	8.30E-01	NA
3(µmol)	2.33E-03	2.33E-03	6.40E-06	2.43E-01	2.55E-01

To summarize, in interphase chromatin two distinct clusters of lifetimes were observed in the phasor plot with distinguished parameters and characteristics suggesting that the probe had different binding model at different concentrations. These two distinct binding behaviors can be explained by the difference in size, softness, and accessibility of the chromatin at the binding regions. The first cluster comprised three concentration 0.05µmol, 0.2µmol and 0.4µmol and has a significantly higher lifetime, which increases as the concentration is increased. This significantly higher and increasing lifetime indicate that the probe is binding to more rigid and

wider regions of chromatin. Rigid, wide minor grooves are the characteristics of CG and GC base pair regions. Given that CG is less rigid than GC, it can be concluded that the probe first binds the less rigid CG and then the most rigid GC regions. This preferential binding to CG and GC base pair regions could simply be due to the wider size of the minor grooves in these regions. However, it is possible that chromatin conformation is such that these regions are more easily and readily accessible to the probe. Moreover, there could be other mechanisms, such as electrostatic potential or other biochemical forces, causing CG and GC regions to be more available for binding. The second cluster, which includes three groups with probe concentrations of 1.0µmol 2.0µmol and 3.0µmol, has a significantly shorter lifetime compared with the first cluster. Despite this significant decrease in the lifetime from 0.4µmol to 1.0µmol of Hoechst 33342, there is no quenching, as there is no significant decrease in the intensity values. These observations suggest that the probe is binding to a softer region. Moreover, the standard deviation of average lifetime is an order magnitude larger in this cluster, indicating larger variability in the softness of the binding sites. Softness, deformability, and instability are the hallmark of AT-rich regions. Therefore, it can be concluded that in the second cluster, the probe is binding to minor grooves rich in AT and TA base pairs. The lifetime is significantly lower because the region is softer, and the energy of the excited probe is used to deform the surrounding, quenching the molecule back to the ground state much faster. The reason why the probe does not readily bind AT regions and prefers GC pairs could be that these regions are less accessible due to chromatin local conformation or the smaller dimensions of the grooves in these regions. However, other biochemical mechanism could be driving the probe to preferentially bind GC regions first.

4.1.2 Metaphase Chromatin

Similar experiment was done on 68 metaphase Hela cells to examine differences and similarities between interphase and metaphase chromatin structure and mechanical properties.

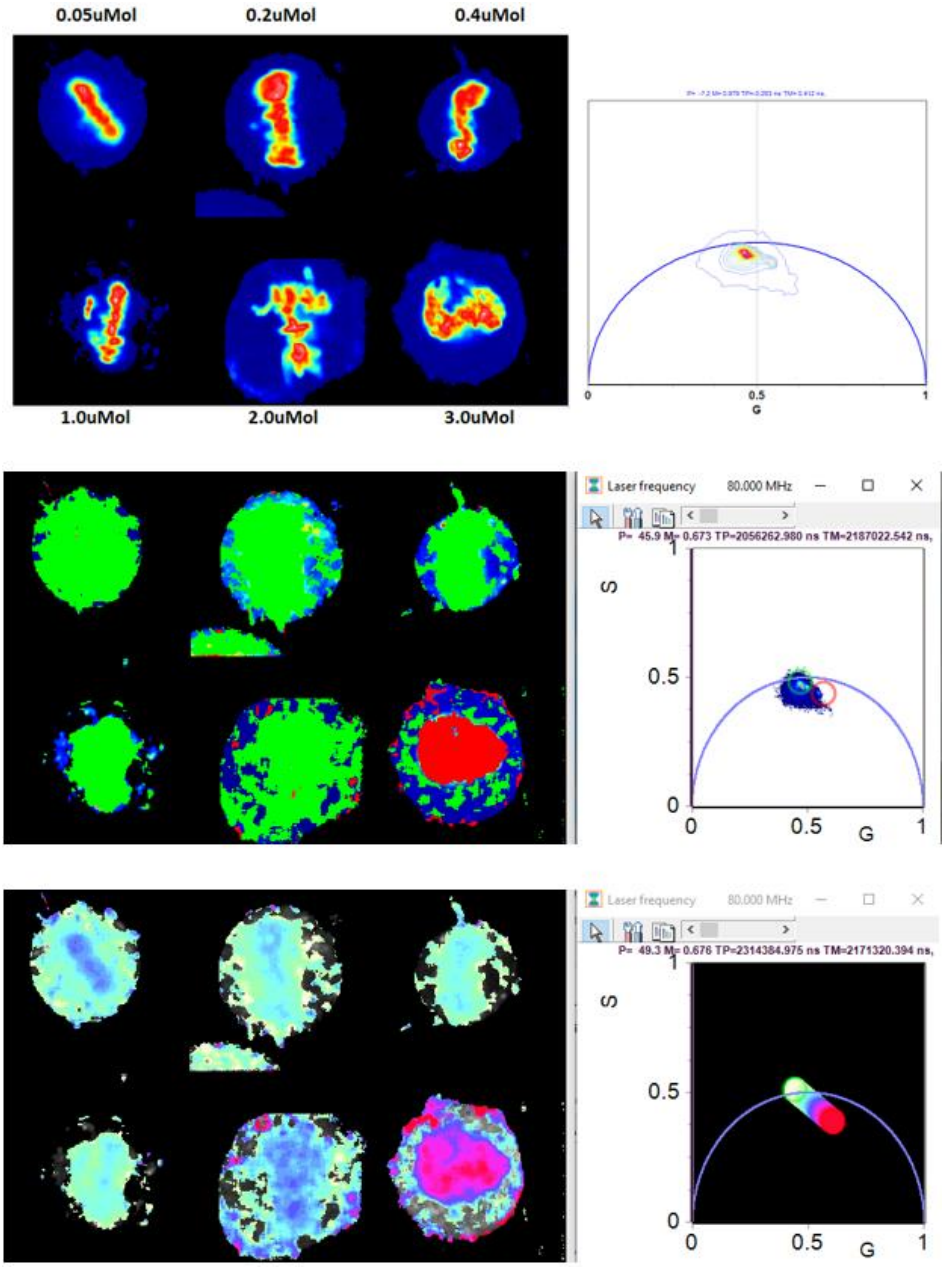

Figure 25: Phasor plot and pseudo-color trajectory showing the shift in the lifetime values in metaphase chromatin.

The phasor plot reveals a linear shift toward shorter lifetime as more Hoechst 33343 was added to the nucleus. It is evident that metaphase chromatin follows approximately the same binding behavior as interphase chromatin. However, the lifetime trajectory of metaphase chromatin is longer than interphase chromatin. To explain metaphase chromatin binding behavior, binding sites' dimensions and compaction and local conformations lifetime values are statistically analyzed.

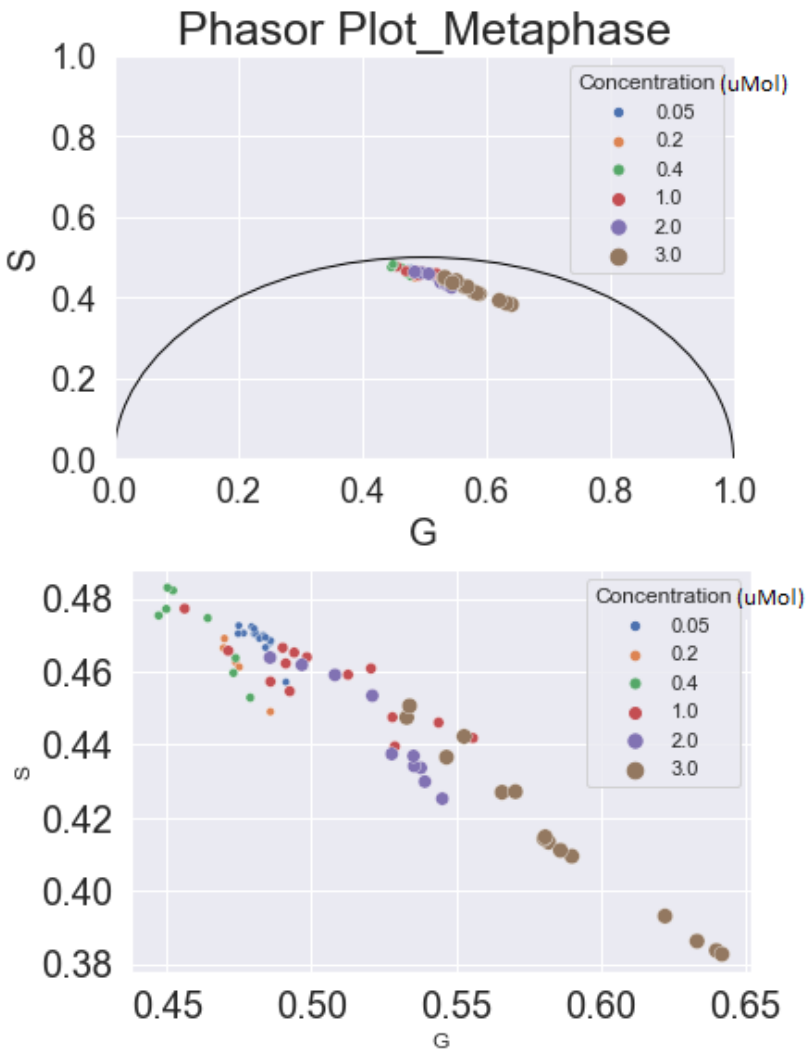

Figure 26: Phasor Plot for Metaphase Chromatin, the bottom phasor is the zoomed-in and show the linear trend of lifetime increase as the concentration of Hoechst 33342 increases

Much like in interphase, metaphase chromatin produces two clusters of lifetime population. The underlying binding mechanism characterizing each cluster seems to be nearly similar in both metaphase and interphase. In the first population, the lifetime increases as the concentration of the probe is increased from 0.05µmol to 0.4µmol, and the lifetime trajectory is almost the same as the interphase lifetime trajectory, shown in Figure 27.

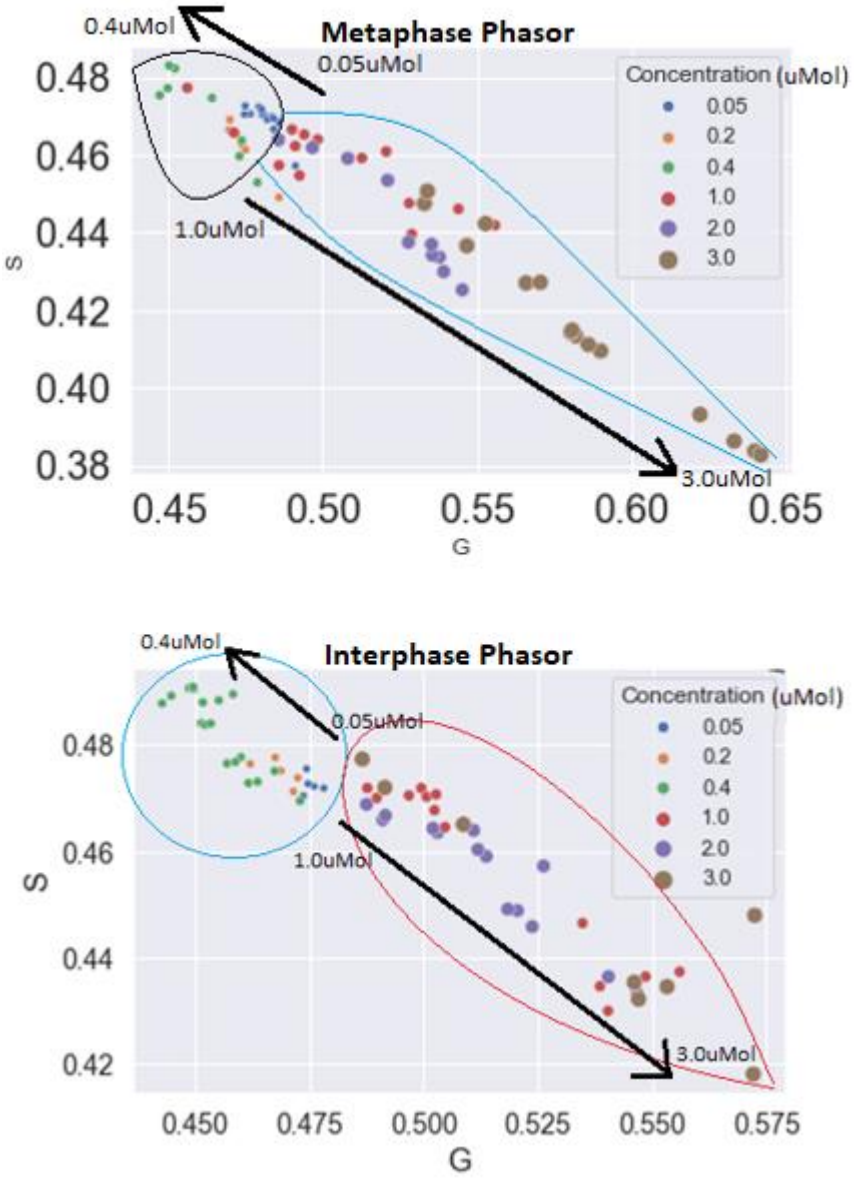

Figure 27: Clustering behavior of metaphase vs interphase chromatin

The second cluster has slightly different characteristics. Most notably is the larger shift in the phasor trajectory in metaphase chromatin as the concentration of the probe is increased from 1.0µmol to 30.0µmol. The significance and interpretation of the phasor behavior is further investigated using statistical analysis of the lifetime and intensity values. There is significant reduction in intensity values as the concentration is increased to 2.0µmol and 3.0µmol, shown in Figure *28*. Therefore, there is quenching in metaphase chromatin at high concentrations of Hoechst 33342. Quenching at these concentrations suggests that the dimensions of the minor grooves in metaphase are reduced compared with interphase. However, not all minor grooves are getting more condensed, only those regions that bind last, which, as will be explained, are AT regions.

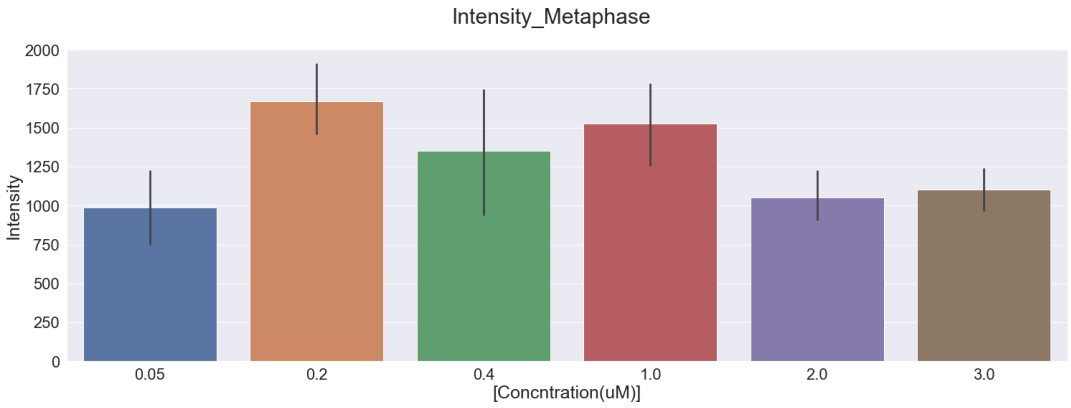

Figure 28: Intensity plot for metaphase chromatin.

In the first cluster, 0.05µmol to 0.4µmol, the average value of phase lifetime and modulation lifetime slightly increases as the concentration of the probe is increased, but the values are not significantly different. However, the average lifetime of the first cluster is significantly higher than of the second cluster. Therefore, much like in interphase chromatin, in metaphase chromatin the probe initially binds to more rigid regions that contain GC and CG base pairs. However, because the lifetime values, more precisely the phase lifetimes, for these three

groups of the first cluster do not increases significantly with increased concentration, as they do in interphase chromatin, it can be concluded that the local conformation of GC-rich regions is more condensed in metaphase chromatin than in interphase chromatin. Figure *29* and Figure *30* show boxplots of modulation and phase lifetime as well as mean and standard deviation values for metaphase chromatin.

Phase Lifetime

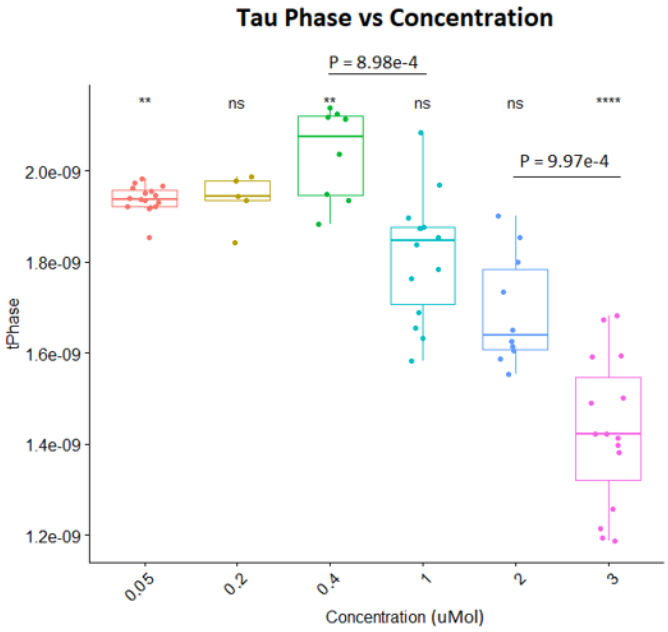

Concentration	N	Mean tau Phase	SD	SE	CI
0.05(uMol)	16	1.94E-09	3.01E-11	7.53E-12	1.61E-11
0.2(uMol)	5	1.94E-09	5.78E-11	2.58E-11	7.18E-11
0.4(uMol)	8	2.04E-09	1.02E-10	3.60E-11	8.50E-11
1(uMol)	14	1.81E-09	1.38E-10	3.68E-11	7.95E-11
2(uMol)	10	1.69E-09	1.22E-10	3.84E-11	8.70E-11
3(uMol)	15	1.43E-09	1.64E-10	4.25E-11	9.11E-11

Figure 29: Phase lifetime values for metaphase chromatin at different concentrations of Hoechst 33342

Modulation Lifetime

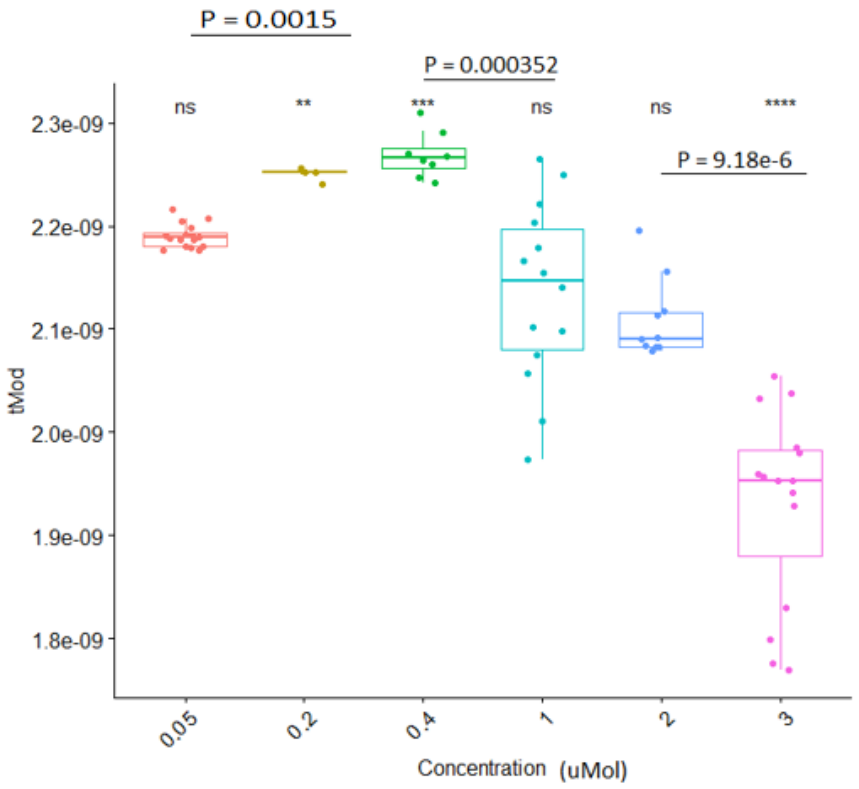

Concentration	N	Mean tau Mod	SD	SE	CI
0.05(uMol)	16	2.19E-09	1.15E-11	2.87E-12	6.11E-12
0.2(uMol)	5	2.25E-09	5.58E-12	2.50E-12	6.93E-12
0.4(uMol)	8	2.27E-09	2.25E-11	7.95E-12	1.88E-11
1(uMol)	14	2.14E-09	8.73E-11	2.33E-11	5.04E-11
2(uMol)	10	2.11E-09	3.86E-11	1.22E-11	2.76E-11
3(uMol)	15	1.93E-09	9.35E-11	2.41E-11	5.18E-11

Figure 30: Modulation lifetime values for metaphase chromatin at different concentrations of Hoechst 33342

Furthermore, statistical analysis revealed that in the second cluster, with concentrations of 1.0µmol to 3.0µmol, the lifetime was not only significantly lower, but both phase and lifetime values significantly decreased as the concentration of the probe was increased. These findings

provide mounting evidence that the binding mechanism for the second cluster is such that the probe binds more softer AT-rich regions. Moreover, the reduction in intensity values suggesting quenching in the second cluster indicate that these regions are more condensed compared with AT regions in interphase chromatin because there is no quenching in interphase chromatin. The AT-rich regions are softer and more deformable compared with GC-rich regions. Therefore, it is more likely that they become more condensed, with dimensions of the minor grooves getting smaller, during metaphase. Whereas GC regions are more rigid and harder to condense. The results of statistical significance are presented in Table 3 and Table 4

Table 3: p_values for statistical significance between Tau Phase among all 6 concentrations

Concentration	0.05(µmol)	0.2(µmol)	0.4(µmol)	1(µmol)	2(µmol)
0.2(µmol)	6.50E-01	NA	NA	NA	NA
0.4(µmol)	5.37E-02	1.37E-01	NA	NA	NA
1(µmol)	2.45E-03	5.37E-02	8.98E-04	NA	NA
2(µmol)	1.31E-04	4.00E-03	2.74E-04	5.37E-02	NA
3(µmol)	1.73E-05	3.22E-04	2.04E-05	1.73E-05	9.97E-04

Table 4: p_values for statistical significance between Tau Modulation among all 6 concentrations

Concentration	0.05(µmol)	0.2(µmol)	0.4(µmol)	1(µmol)	2(µmol)
0.2(µmol)	1.51E-03	NA	NA	NA	NA
0.4(µmol)	2.51E-04	0.0999001	NA	NA	NA
1(µmol)	5.05E-02	0.00623495	3.52E-04	NA	NA
2(µmol)	6.22E-04	0.000999001	1.37E-04	3.71E-01	NA
3(µmol)	1.16E-05	0.000276426	1.53E-05	1.16E-05	9.18E-06

4.1.3 Comparing Interphase and Metaphase Chromatin

Examining the binding behavior of the probe in interphase and metaphase chromatin reveals valuable information about the size, softness/deformability and accessibility of chromatin

structure and conformation. In both interphase and metaphase chromatin, two distinct binding behavior are observed. Using phasor plot analysis, lifetime values for each cluster are investigated. The result suggests that at low concentrations, in both metaphase and interphase chromatin, the probe preferentially binds the more rigid areas of the chromatin. It is because these regions tend to have wider minor grooves. However, it is also possible that these regions are more accessible due to the local conformation of chromatin. As the concentration is increased and the GC regions are filled, the probe begins binding softer and more deformable regions that are rich in AT base pairs. This is because AT regions tend to have narrower minor grooves. It is also possible that these regions are less accessible due to local conformation of chromatin.

It is worth noting, however, that in the first three addition of Hoechst 33343, going from 0.05µmol to 0.4µmol, where the probe is binding GC regions, the highest concentration is 0.4µmol of Hoechst 33342. Whereas in the binding regime associated with AT regions another 2.6µmol of the probe binds with AT minor grooves. Therefore, given the fact that AT associate minor grooves are narrower than GC-rich minor grooves, it can be concluded that there are far more AT regions available for binding than GC regions. This finding is further confirmed by statistical analysis of lifetime values of interphase and metaphase chromatin. As shown in Table *5*, the lifetime values of GC associated binding regions are significantly different between interphase and metaphase chromatin. This is because in metaphase the chromatin structure becomes more condensed, reducing the size of minor grooves. Since there are much less GC sites available, when they are condensed, it significantly affects the lifetime. On the other hand, the AT associated lifetime values in metaphase and interphase only differ in the last group with highest concentration. In other words, there is no significant difference between the lifetime values in metaphase and interphase chromatin as the concentration of Hoechst 33342 is increased

from 0.04 to 2µmol. The effect of chromatin condensation in AT regions are only evident when the probe concentration is at 3.0µmol. Therefore, it can be confirmed that there are far more AT-rich minor grooves available for binding, making the effect of chromatin condensation during metaphase less significant compared to GC-rich regions. Figure 32 shows the lifetime values of metaphase and interphase chromatin in the same plot.

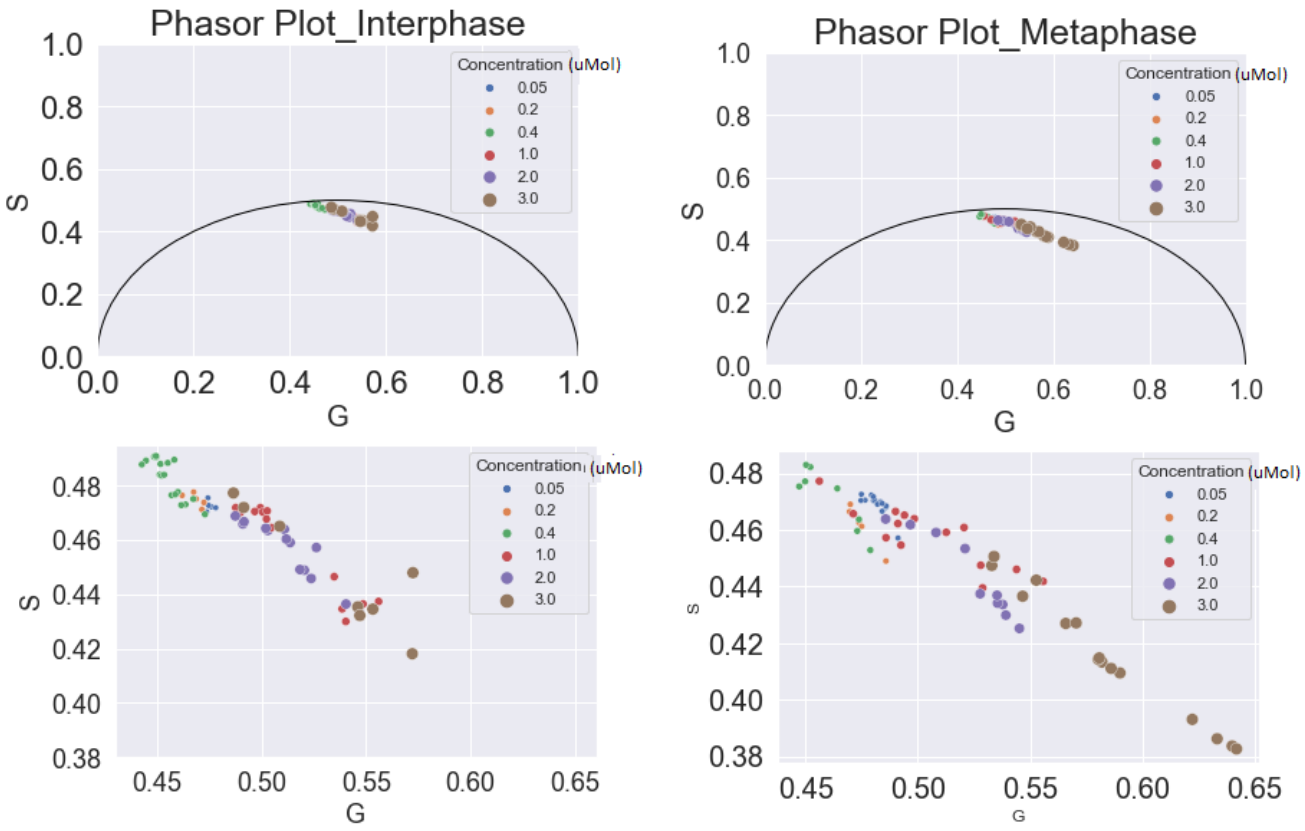

Figure 31: Phasor plot of metaphase and interphase chromatin

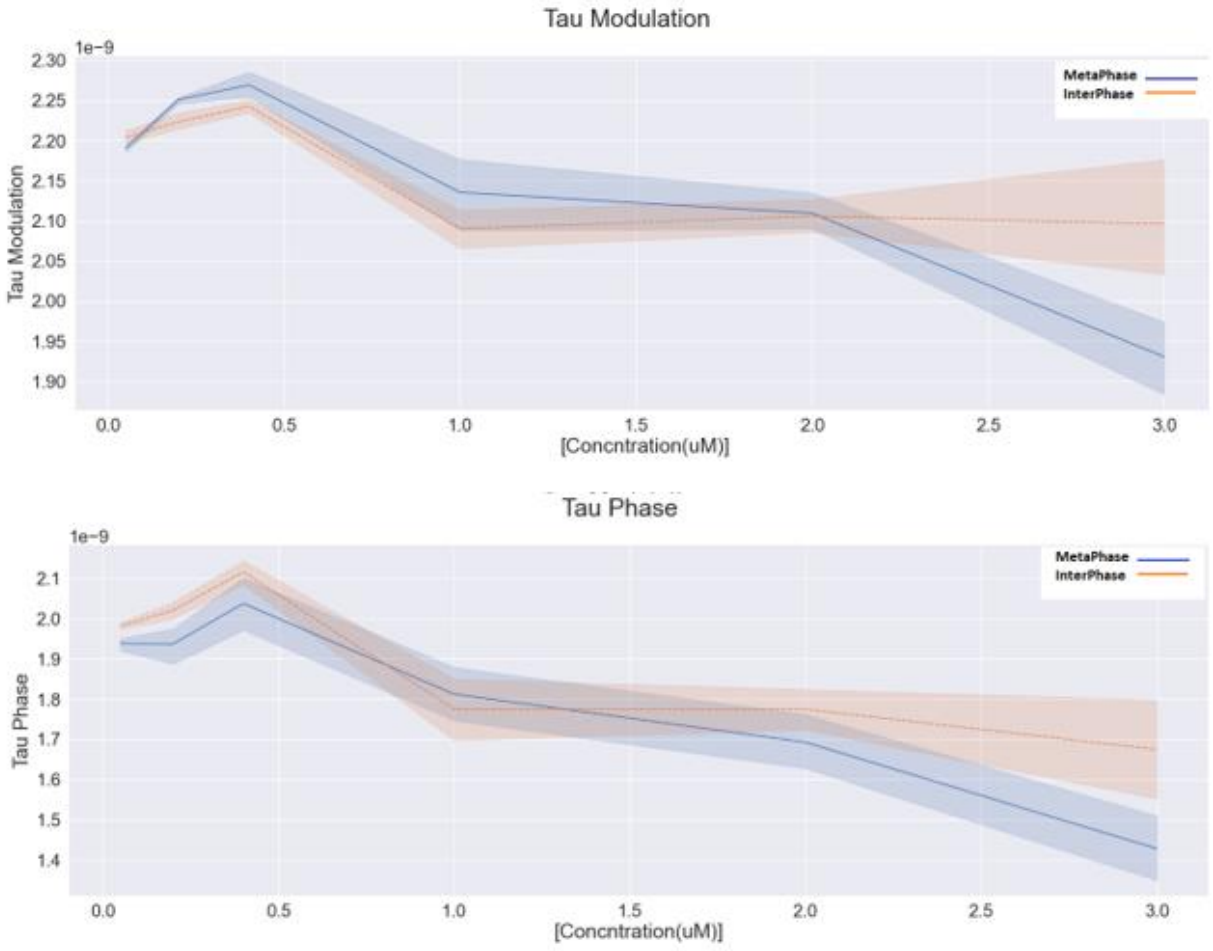

Figure 32: Comparing lifetime values of metaphase and interphase chromatin

Table 5: Statistical significance between lifetime values of interphase chromatin vs metaphase chromatin at different concentrations of Hoechst 33342. Orange indicates concentrations at which lifetime is significantly different between metaphase and interphase chromatin.

Concentration	P-Values for Tau Modulation	P-Values for Tau Phase
0.05(µmol)	2.86E-02	3.36E-03
0.2(µmol)	1.59E-02	7.94E-03
0.4(µmol)	7.63E-03	4.07E-02
1(µmol)	1.55E-01	7.93E-01
2(µmol)	7.09E-01	1.72E-01
3(µmol)	3.92E-04	1.30E-02

4.2 Conclusion and Discussion

Examining the lifetime and binding behavior of Hoechst 33342 to chromatin were used to get insight into local structure of chromatin namely the size, softness/stiffness, and accessibility of the minor grooves. Phasor plot and lifetime values of Hoechst 33342 at different concentrations reveals that GC-rich regions have minor grooves with larger dimensions and more rigid structures. Therefore, due to their larger size, the probe binds to these regions first. Moreover, due to rigidity of chromatin local structure in these regions, at lower concentrations, when the probe is binding to GC-rich minor grooves, the lifetime is significantly longer. On the other hand, AT-rich regions are associated with narrower and softer minor grooves. Significantly shorter lifetime at higher concentrations confirms the small and deformable structure of minor grooves in these regions compared with GC regions.

Finally, there is a significantly pronounced difference between lifetime values of interphase chromatin and metaphase chromatin at low concentrations. This difference is due to the fact that GC-associated binding grooves are condensed during metaphase. However, lifetime in AT-rich minor grooves significantly changes between metaphase and interphase only at the highest concentration of the probe, namely at 3 micro-mol of Hoechst 33342. Below this level there is no significant difference in lifetime values between metaphase and interphase. A very likely explanation for this behavior is that the local conformation of metaphase chromatin is such that there are far more AT-rich regions available and accessible for binding compared with interphase chromatin. Therefore, during metaphase, the effect of chromatin condensation on the lifetime is significant for GC-minor grooves because they get condensed into smaller-sized grooves. The abundance of accessible AT-minor grooves during metaphase offsets the effect of metaphase condensation on the lifetime of Hoechst in these regions. However, at very high concentrations

of the probe in metaphase chromatin, when all available AT-minor grooves are filled, the lifetime significantly drops below that of interphase chromatin. Schematics of DNA structure and the minor grooves at interphase and metaphase chromatin are shown in Figure *33*. In this figure, green spots are GC base pairs that lead to wider and more rigid grooves, and blue spots are AT base pairs corresponding to wider, softer, and more accessible minor grooves. There are more AT-associated minor grooves available and accessible for binding in metaphase chromatin than there are in interphase. However, the number of accessible GC-associated minor grooves is approximately the same in metaphase and interphase chromatin.

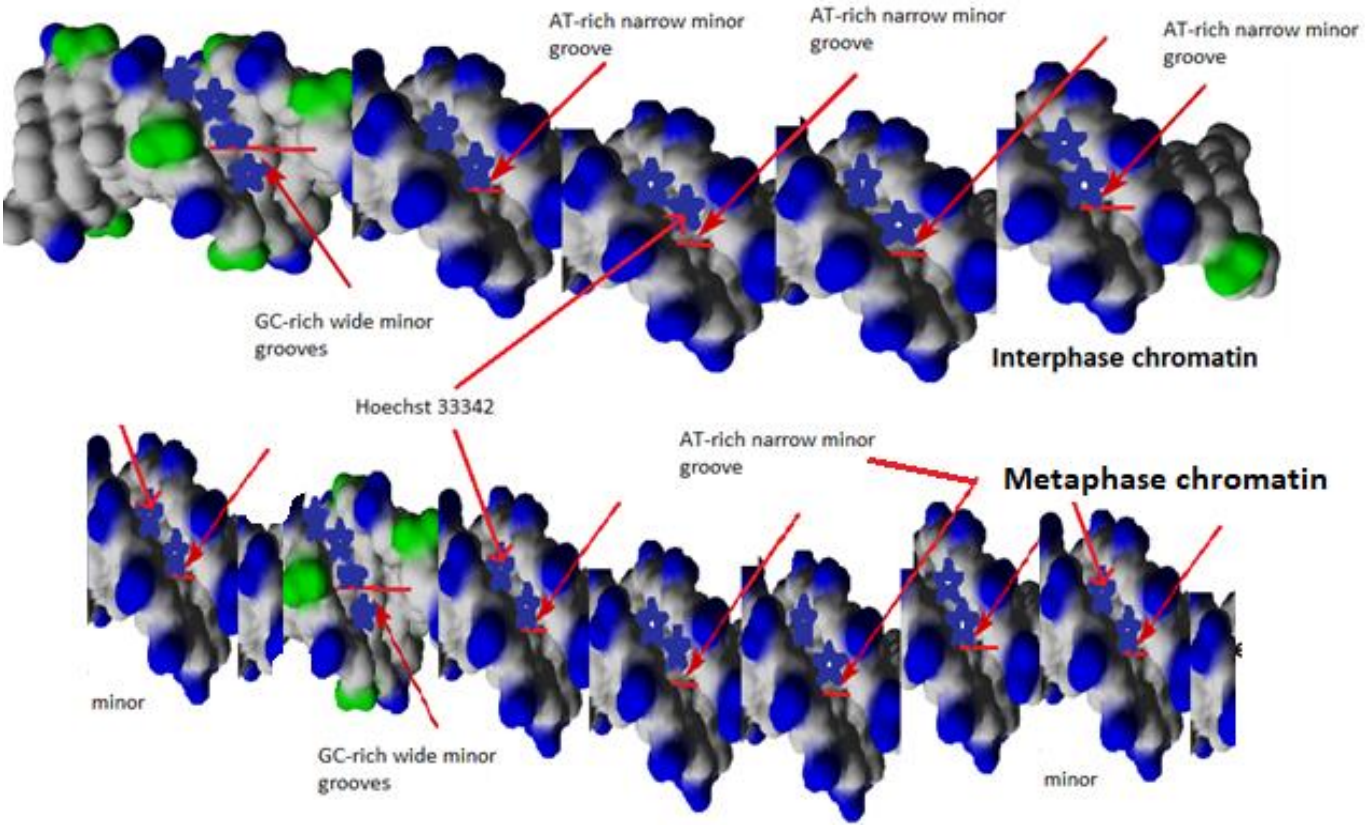

Figure 33: Schematic of DNA structure and minor grooves at interphase and metaphase chromatin. In metaphase chromatin, there are more AT-rich, narrow minor grooves available for binding than there are in interphase chromatin.

Chapter Five: Chromatin in Metastatic Tumors

The primary objective of this experiment was to study Hoechst 33342 lifetime and its variation to report on softness or stiffness and deformability or rigidity of chromatin and to examine any correlation between nuclear and chromatin softness and deformability. Neither the cause of nuclear softness and deformability nor its effect on the mechanobiology of nuclear components such as chromatin is well understood. Recent studies suggest that nuclear softness and deformability are two mechanisms that facilitate and accelerate spread of cancer cells from tissue to the blood stream and throughout the body. Therefore, the most aggressive metastatic cancer cells are expected to have softer and more deformable nuclei compared with non-malignant tumor cells or tumor cells that do not metastasize or spread at a slower rate. In this research, three different types of breast cells with different tumorigenic characteristic and levels of aggressiveness are studied. These cell lines are: MCF10A, MCF7 and MDA-MB231. The most aggressive and invasive cell type in this selection is MDA-MB231, which is expected to have the softest and most deformable nucleus, and MCF10A, which is a non-malignant epithelial cell line is expected to have a stiff and rigid nucleus. All the cells are labeled with different concentrations of Hoechst 33342 nuclear dye. The concentrations under study are 0.4 µmol, 1.0 µmol, 2.0 µmol and 3.0 µmol of Hoechst 33342. The labeled cells are imaged and FLIM measurements are collected. To detect and report on softness of chromatin, lifetime of Hoechst at each concentration is compared between three different cell types. To investigate deformability of chromatin, changes in the lifetime of Hoechst in each individual cell line is examined at increasing concentrations of the probe.

5.1 Results

MCF10A, MCF7 and MB231 cells were initially labeled with 0.4 µmol of Hoechst. At this concentration, as shown in Figure *34*, the phasor plot revealed that MB231 had a different lifetime than MCF10A and MCF7. The phasor for MB231 was shifted toward shorter lifetime.

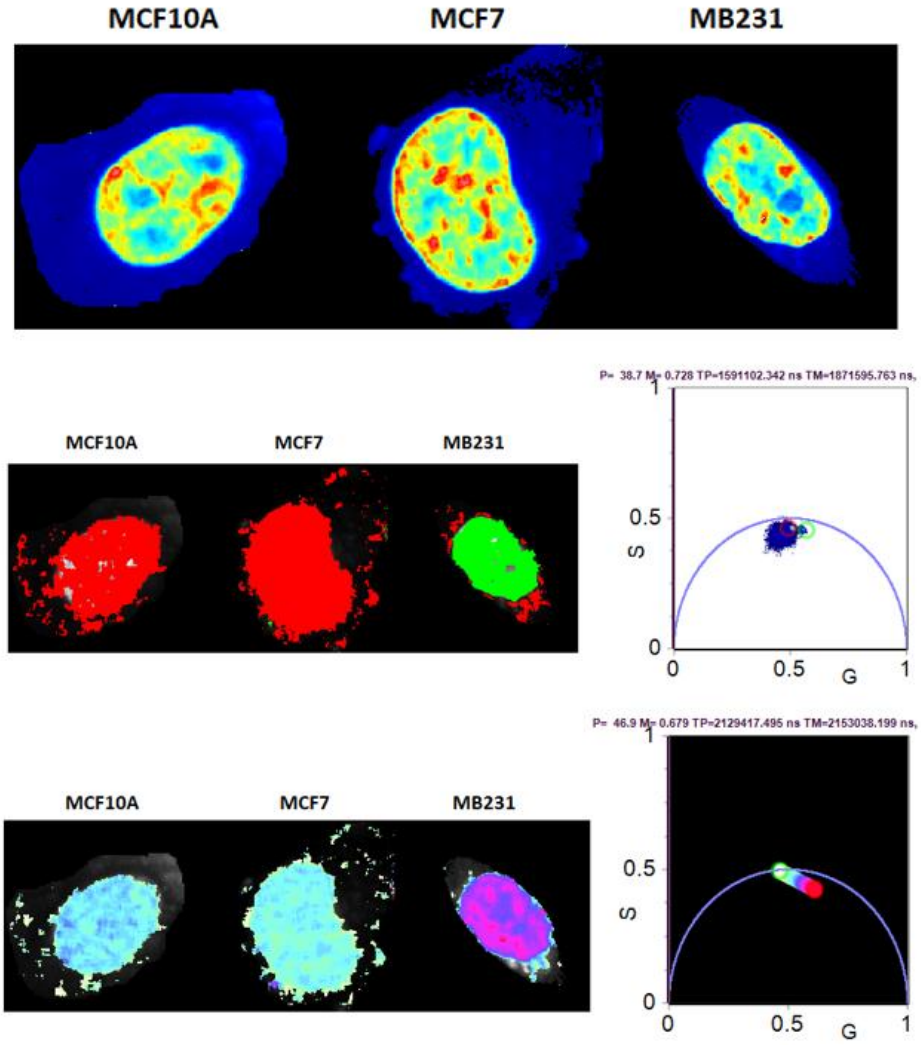

Figure 34: Three types of tumor cell labeled with 0.4 µmol of Hoechst 33342. The lifetime trajectory and pseudo-coloring show MB231(the most aggressive of the three) has a shorter lifetime than the other two.

Concentration of Hoechst was then increased to 1.0, 2.0 and 3.0 µmol in all three cell types. The lifetime trajectories of Hoechst at all 4 concentrations in each cell line is shown in Figure *35*. For quantitative and statistical analysis, average values of modulation lifetime and phase lifetime for each cell was calculated. The phasor plots in Figure *36* show the average phasor position for each cell. In MB231 cells, the phasor trajectory follows a linear shift toward shorter lifetime as the concentration is increased from 0.4µmol to 2.0µmol. Moreover, at these concentrations, there was a clear variability in lifetime behavior of Hoechst. Beyond that concentration, 2.0µmol, the lifetime of Hoechst was suddenly increased its concentration was increased from 2.0µmol to 3.0µmol, and the variability in lifetime was reduced as there was a clear clustering of 3.0µmol cells seen in the phasor plot. In MCF7 cells, lifetime of Hoechst consistently decreased as its concentration was increased. As shown in the phasor plot, MCF7 cells labeled with 0.4µmol of Hoechst show a distinctly different lifetime than other populations of MCF7 with higher concentrations of Hoechst. This population, MCF7 with 0.4µmol of Hoechst, showed lifetimes similar to MCF10A with the same concentration of Hoechst. Qualitative analysis of phasor plots indicated that Hoechst at low concentrations had almost the same lifetime behavior in MCF7 and MCF10A, which was different from that of MB231. Statistical analysis was done to quantitatively investigate these similarities and differences between different cell types and at different concentrations of Hoechst.

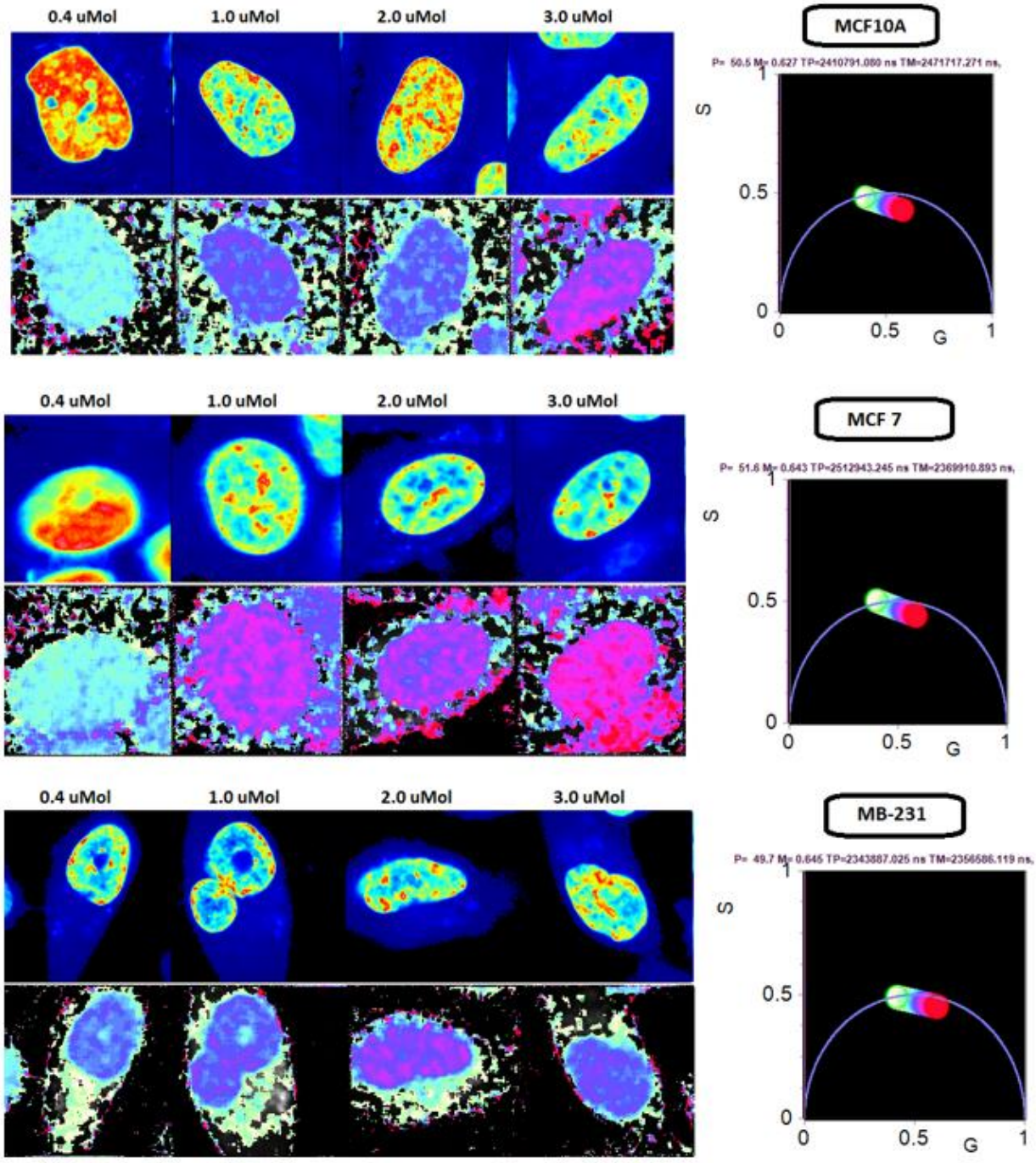

Figure 35: All three cell types labeled with different concentrations of Hoechst 33342.

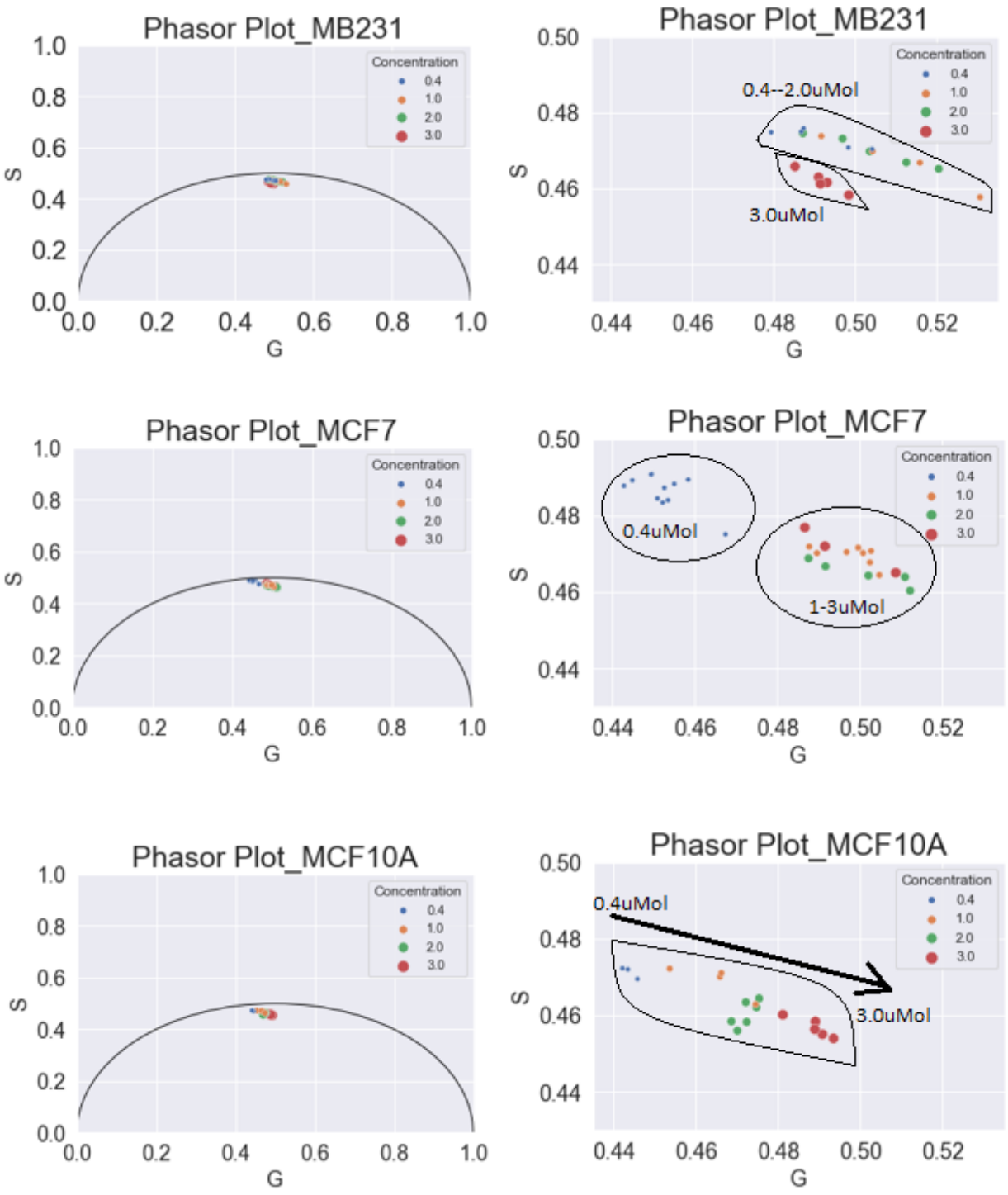

Figure 36: Average lifetime values for each cell. The length of the lifetime trajectory is longer in MCF7. There is a clear shift in MB231 trajectory compared with MCF10A.

Plots of phase and modulation lifetime for each cell line and different concentrations of Hoechst are shown in Figure 37. Over all, both phase and modulation lifetime values showed that in MB231 cells, Hoechst had a smaller lifetime than MCF7 and MCF10 had smaller lifetime than MCF10A. The only exception was at very high concentration of Hoechst, namely at 3.0µmol. At this concentration, the lifetime of Hoechst in MB231 was larger than in MCF7 and almost similar to MCF10A. The average modulation lifetime of Hoechst in MB231 cells increased from 2.0e-9±6.84e-11 seconds at 2.0µmol of Hoechst to 2.18e-9±9.99e-12 seconds at 3.0µmol of Hoechst. That means the lifetime increased by 0.18e-9 seconds and the statdanrd deviation decreased 5.48e-11. The increase in lifetime in MB231 cells suggests that the minor grooves are stretched open as more Hoechst is added to chromatin. One reason for widening of minor grooves in MB231 cells at high concentrations of Hoechst could be excessive softness of chromatin in these cells. The lifetime of Hoechst in MCF7 and MCF10A, however, continued to decrease as its concentration was increased. A logical conclusion is that chromatin in these cells are not as soft as in MB231 cells.

Another observation is that the standard deviation of lifetime values in MB231 increased as the concentration of Hoechst was increased from 0.4µmol to 2.0µmol. But beyond that point, the stabdard deviation was decreased as the concentration was increased and the grooves were streched open. Larger standard deviation at lower concentrations indicate variability in minor grooves dimensions. This observations suggest that the minor grooves may be differentially deformed depending on how much Hoechst is binding each groove. The minor grooves with less probe binding them have smaller sizes and therefore shorter lifetime. And the minor grooves with more probes binding them are slightly streched open and have longer lifetime compared to less populated grooves. At very high concentration, the minor grooves are more evenly

populated with Hoechst and therefore more evenly streched open. As a result, there is less variation in the lifetime values and the standard deviation is decreased as the lieftime is increased.

Figure 37: Plots of modulation and phase lifetime for all three tumor cell types.

The summary of modulation and phase lifetime values and other statistics including sample size, standard deviation and standards errors for all three cell lines at all concentration groups are tabulated in Table 6and Table 7. Standard deviation of lifetime values in MCF10A cells do not change much as they do increases consistently in MCF7, suggesting less deformability of MCF10A cells compared to MCF7 cells. Changes in standard deviation of lifetime is also noticeable in MB231 cell, as discussed earlier, higher degree of deformability on these cells. For further investigation of deformability, the behavior of each cell line and its

associated lifetime and changes in the lifetime of Hoechst with respect to changes in its concentration is studied and analyzed.

Table 6: Summary of Modulation lifetime values and statistics

Cell Type	Concentration (µmol)	N	Tau Modulation(s)	SD	SE	CI
MCF10A	0.4	3	2.34E-09	2.33E-12	1.35E-12	5.79E-12
MCF10A	1	4	2.26E-09	2.38E-11	1.19E-11	3.79E-11
MCF10A	2	6	2.27E-09	2.38E-11	9.74E-12	2.50E-11
MCF10A	3	5	2.21E-09	1.14E-11	5.09E-12	1.41E-11
MCF7	0.4	10	2.24E-09	1.76E-11	5.56E-12	1.26E-11
MCF7	1	8	2.12E-09	2.25E-11	7.96E-12	1.88E-11
MCF7	2	5	2.13E-09	3.62E-11	1.62E-11	4.50E-11
MCF7	3	7	2.04E-09	8.14E-11	3.08E-11	7.53E-11
MB231	0.4	5	2.13E-09	3.30E-11	1.48E-11	4.10E-11
MB231	1	4	2.08E-09	4.54E-11	2.27E-11	7.22E-11
MB231	2	8	2.05E-09	6.84E-11	2.42E-11	5.72E-11
MB231	3	5	2.18E-09	9.99E-12	4.47E-12	1.24E-11

Table 7: Summary of Phase lifetime values and statistics

Cell Type	Concentration (µmol)	N	Tau Phase(s)	SD	SE	CI
MCF10A	0.4	3	2.12E-09	1.70E-11	9.82E-12	4.23E-11
MCF10A	1	4	2.01E-09	5.39E-11	2.69E-11	8.57E-11
MCF10A	2	6	1.95E-09	9.73E-12	3.97E-12	1.02E-11
MCF10A	3	8	1.81E-09	8.75E-11	3.09E-11	7.32E-11
MCF7	0.4	10	2.14E-09	4.70E-11	1.49E-11	3.36E-11
MCF7	1	8	1.88E-09	3.04E-11	1.07E-11	2.54E-11
MCF7	2	5	1.85E-09	5.32E-11	2.38E-11	6.60E-11
MCF7	3	7	1.73E-09	1.61E-10	6.08E-11	1.49E-10
MB231	0.4	5	1.92E-09	4.79E-11	2.14E-11	5.95E-11
MB231	1	4	1.83E-09	8.64E-11	4.32E-11	1.37E-10
MB231	2	8	1.77E-09	1.37E-10	4.84E-11	1.14E-10
MB231	3	5	1.87E-09	2.78E-11	1.25E-11	3.46E-11

Statistical analysis confirms that the modulation lifetime of Hoechst at all concentrations remains significantly shorter in MCF7 cells than in MCF10A cells. In MB231 cells, the modulation lifetime of Hoechst at low and medium concentrations is significantly shorter than in MCF7 and MCF10A cells. However, at high concentration of 3.0µmol of Hoechst, the modulation life in MB231 is significantly longer than in MCF7 and is almost similar to MCF10A. The phase lifetime behavior, however, does not follow the same pattern consistently. The phase lifetime of Hoechst is significantly shorter in MB231 cells only at 0.4µmol and 1.0µmol concentrations. And the phase lifetime in MCF7 is significantly shorter than in MCF10A only at 1.0µmol of Hoechst. Due to lack of consistency in the phase lifetime behavior, only modulation lifetime is considered. It is possible that the modulation lifetime is a more sensitive parameter for detecting softness in the local structure. Boxplots along with statistical significance between each cell types at all concentration are shown in Figure *38* to Figure *41*.

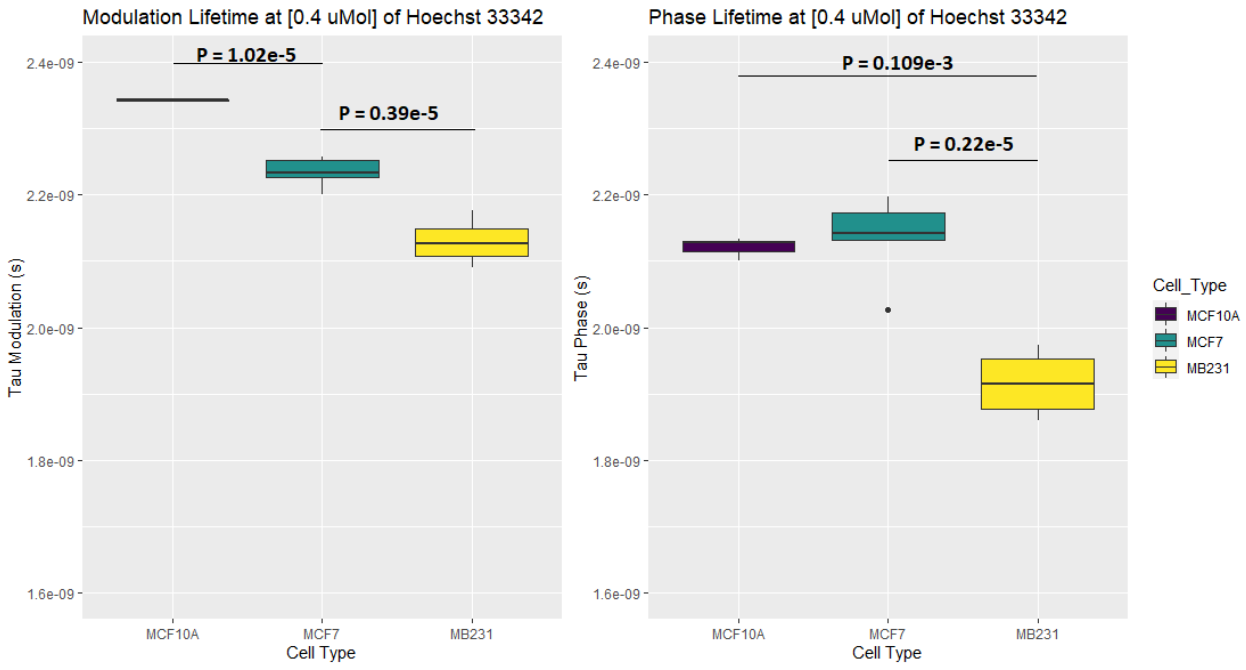

Figure 38: Boxplot and statistical significance between all three cell lines at 0.4µmol of Hoechst.

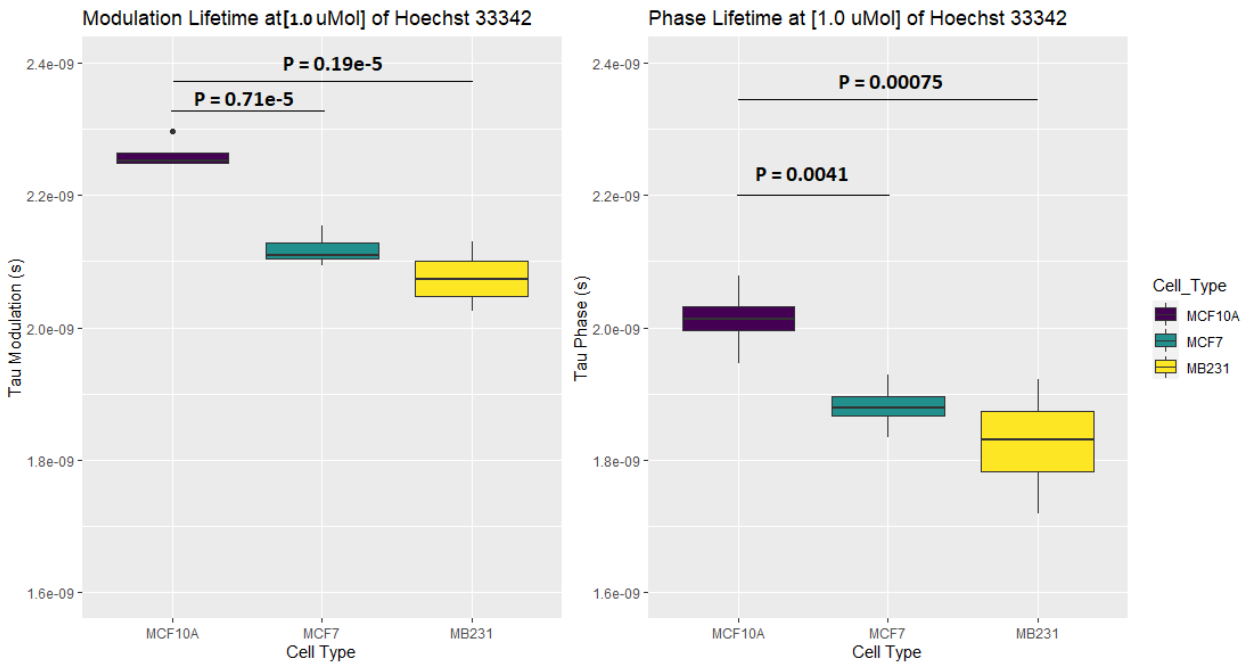

Figure 39: Boxplot and statistical significance between all three cell lines at 1.0µmol of Hoechst.

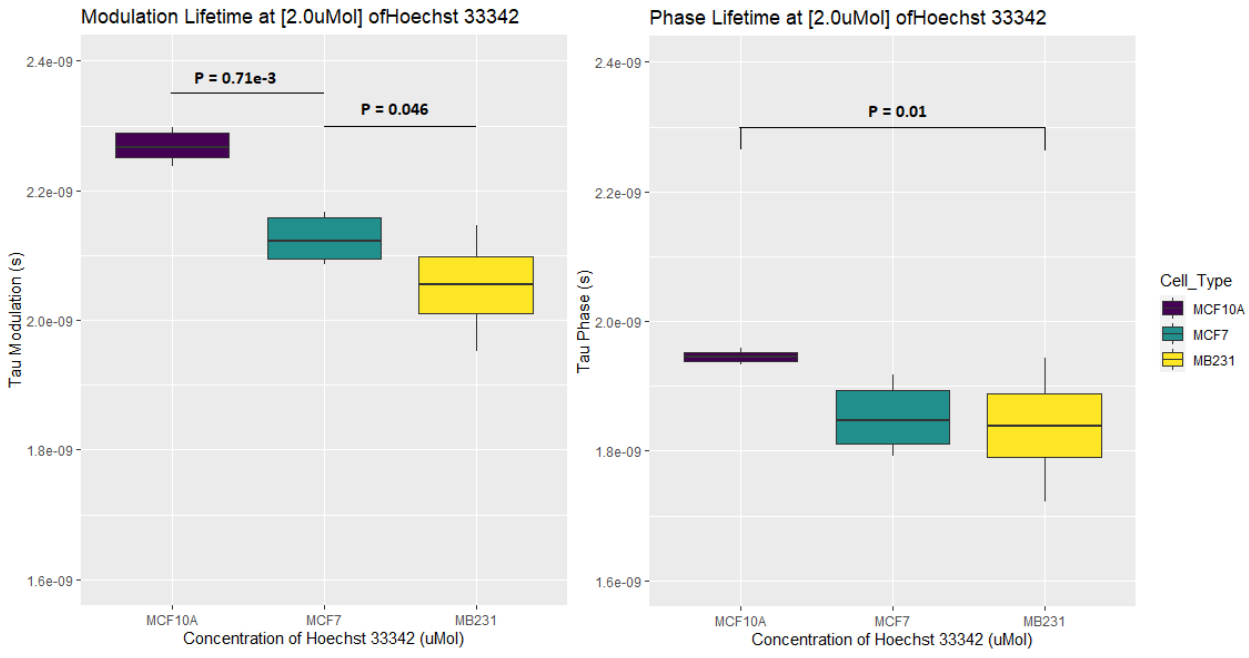

Figure 40: Boxplot and statistical significance between all three cell lines at 2.0µmol of Hoechst.

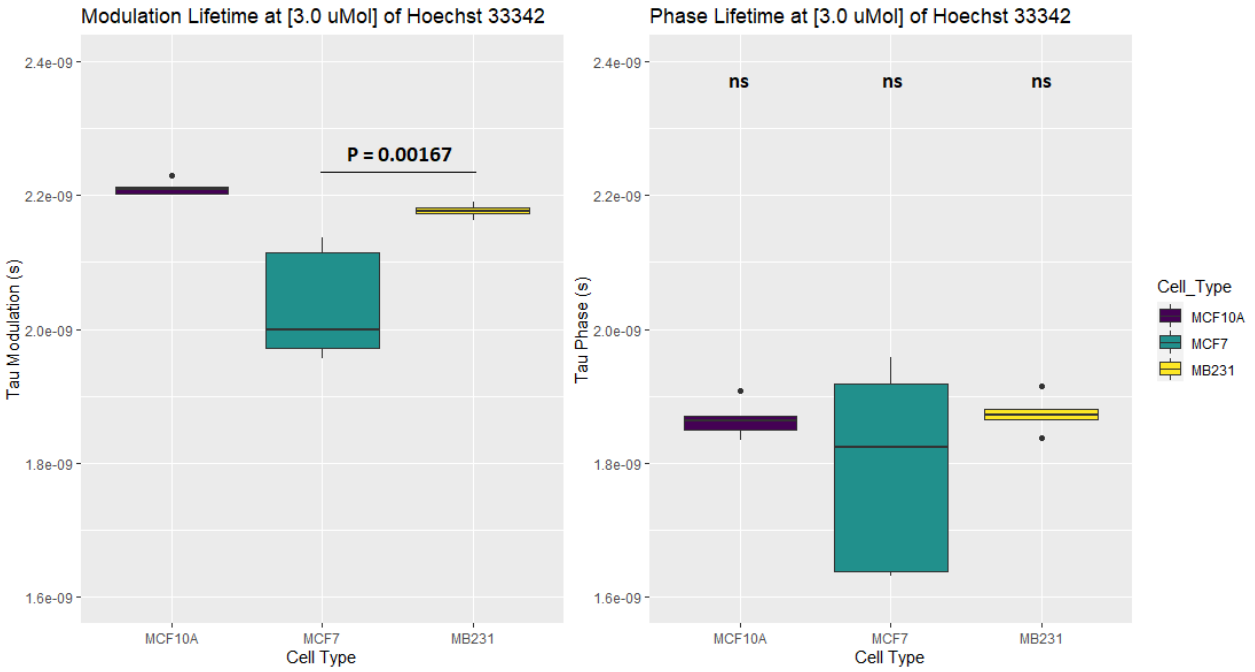

Figure 41: Boxplot and statistical significance between all three cell lines at 3.0µmol of Hoechst.

To investigate deformability of chromatin in different cell lines, as discussed earlier, changes in the lifetime of Hoechst with respect to its concentration is examined in each cell types separately. In MB231 cells, as shown in Figure *42*, the modulation lifetime significantly decreases at the concentration of Hoechst is increased from 0.4µmol to 2.0µmol. This significant decrease in lifetime is partly due to quenching and partly due to the softness of chromatin. It is not clear whether quenching has a larger contribution to the shortening of lifetime or softness. However, in MCF10A, which is the least soft cell line, the modulation lifetime does not significantly change. Therefore, it is very likely that in MB231 at 0.4 to 2.0µmol of Hoechst, softness of chromatin is leading cause of the significant decrease in the modulation lifetime. When the concentration of Hoechst is increased to 3.0µmol, the modulation lifetime significantly

increases, suggesting that the binding grooves are opening wider. The ability for the minor grooves for getting wider is most likely due the deformability of chromatin in MB231 cells.

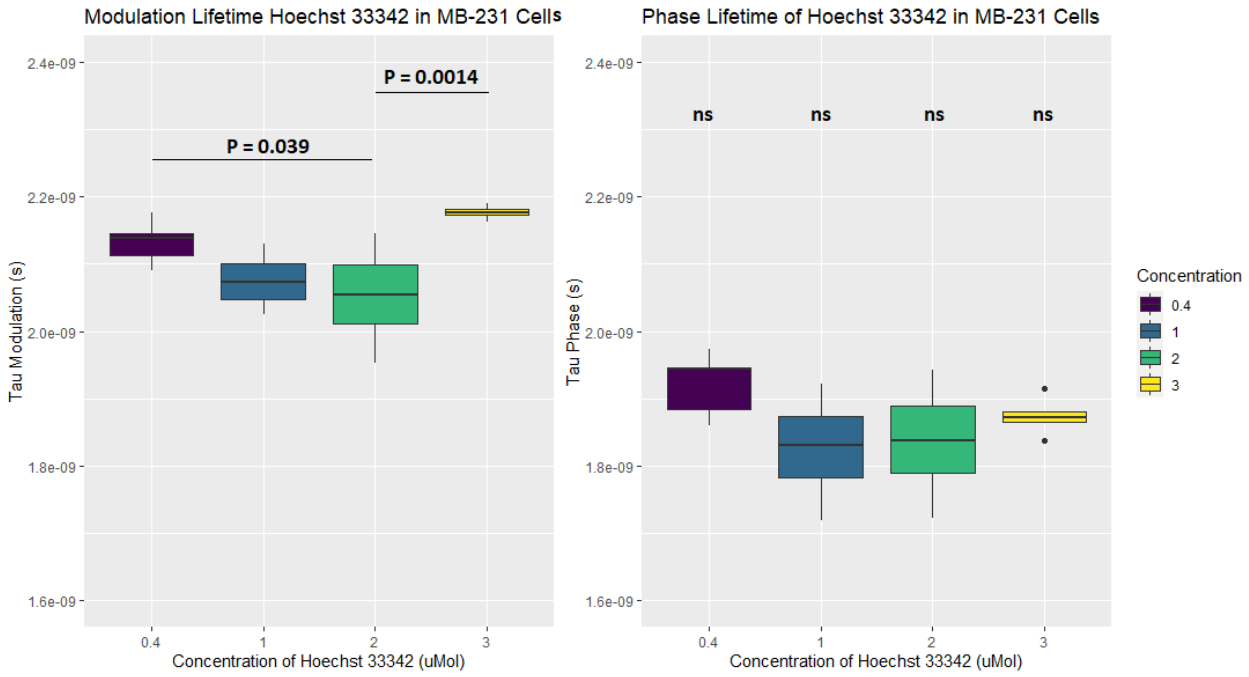

Figure 42: The lifetime of Hoechst at different concentrations in MB231 cells.

MCF7 cells, as shown earlier, are less soft than MB231 but softer than MCF10A since their lifetime is longer than MB231 and shorter than MCF10A. The modulation lifetime of Hoechst in these cells significantly decreases as its concentration increases. Unlike in MB231, the lifetime of Hoechst in MCF7 significantly decreases at the highest concentration, 3.0µmol, of the probe. Therefore, the dimensions of the minor grooves in MCF7 cells at this concentration do not change. As a result, it can be postulated that even though chromatin in MCF7 cells is soft, it is not deformable or at least as deformable as chromatin in MB231 cells. Plots and statistical significance for MCF7 cells are shown in Figure *43*.

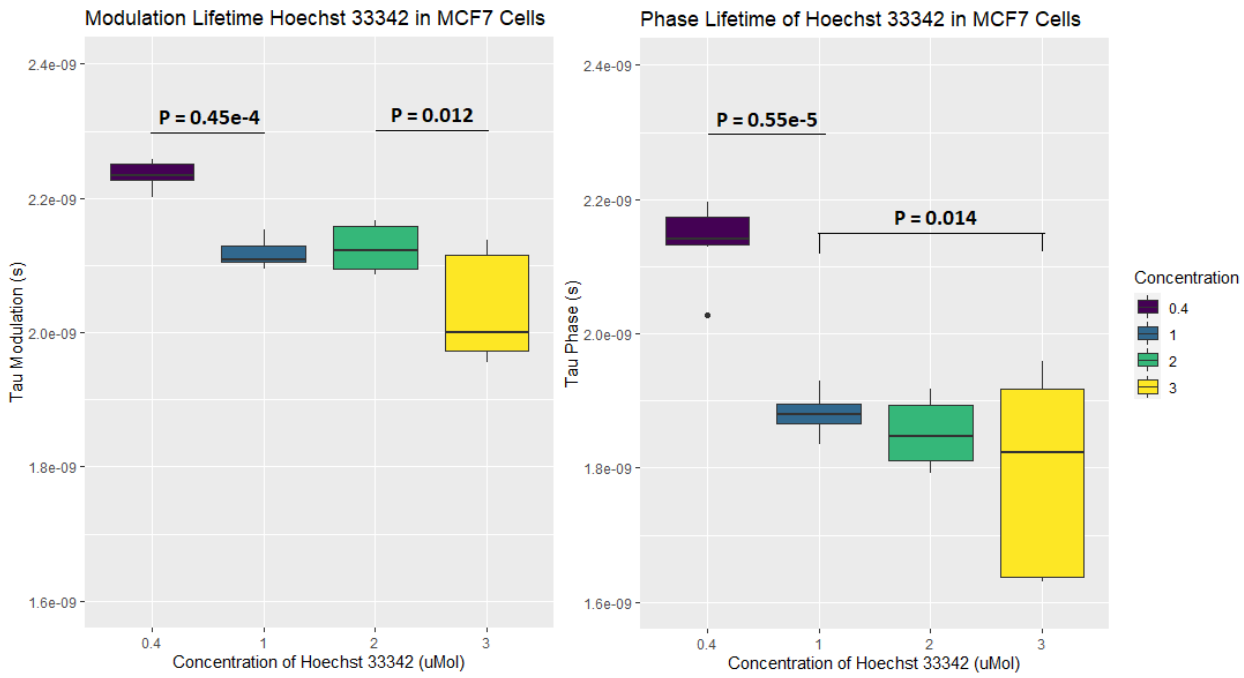

Figure 43: The lifetime of Hoechst at different concentrations in MCF7 cells.

Finally, in MCF10A cells, which have the most rigid nucleus and chromatin, the modulation lifetime of Hoechst does not significantly change as its concentration is increased from 0.4µmol to 2.0µmol. This is expected because the chromatin is not as soft as it is in MB231 or MCF7 cells. The only significant decrease in modulation lifetime happens at 3.0µmol of Hoechst. This decrease in lifetime, therefore, is most likely attributable to quenching effect and not to softness of the environment. The phase lifetime in MCF10A consistently decreases as the concentration of Hoechst increases. However, the phase lifetime values, due to their less consistent behavior, are not the included in the analysis and the final conclusion. The plots and statistical significance for lifetime values in MCF10A are shown in Figure *44*.

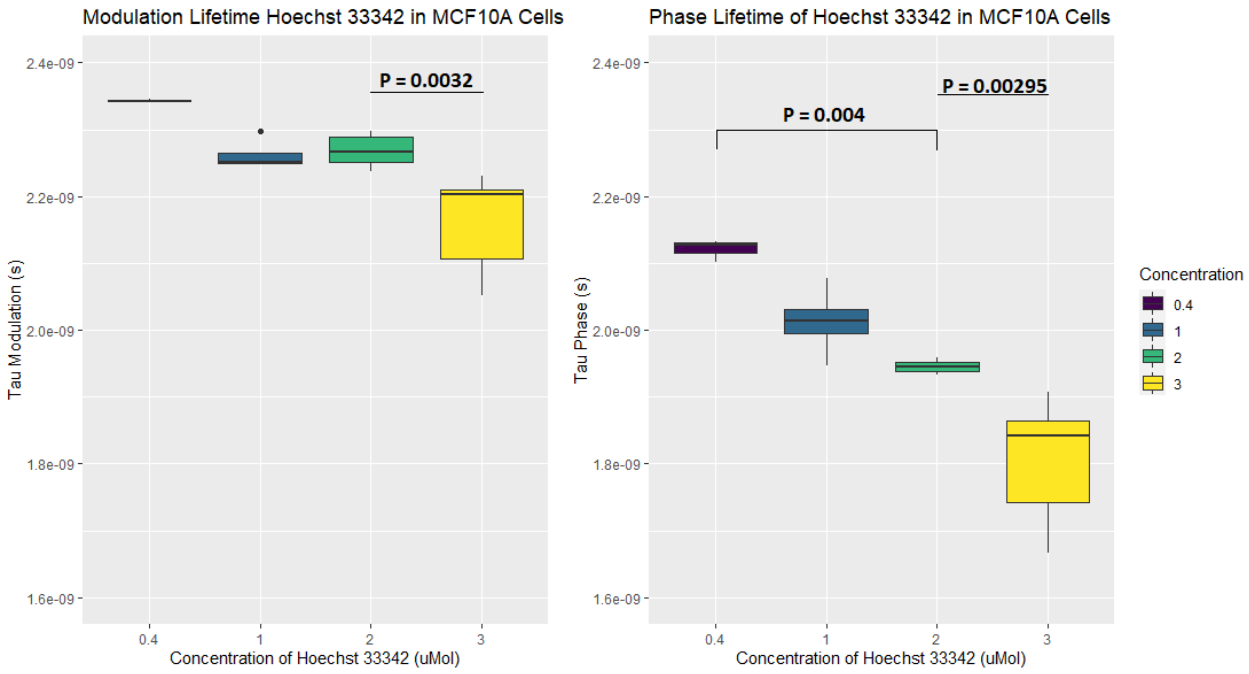

Figure 44: The lifetime of Hoechst at different concentrations in MCF10A cells.

5.2 Conclusion and Discussion

Fluorescence Lifetime Imaging and phasor analysis are powerful techniques that can reveal information about mechanical properties of chromatin such as stiffness and deformability. In this study, the binding behavior of Hoechst 33342 and its lifetime were studied to investigate and report on softness and deformability of chromatin in three different cell lines. MCF10A, MCF7 and MDA-MB231 cell lines were studied in this research. The MCF10A cell are normal breast cells derived from non-tumorigenic epithelial cells. These cells were used as control. The MCF7 cell line is a human breast carcinoma that forms tumors which are able to metastasize into lungs, liver, and spleen, but they are not as invasive as MB231 cells (30). The MDA-MB231 cell line is a triple-negative breast cancer (TNBC) cell type that are highly aggressive and invasive. These cells can metastasize into the bones, brain, and lungs (31).

Comparing the lifetime of Hoechst in these three cell lines showed that at low to medium concentrations, Hoechst has the longest lifetime in MCF10A and the shortest lifetime in MB-231, with the MCF7 lifetime in between the other two cell types. These results postulate that chromatin in MB-231 cells is the softest of all three cell types under investigation. The second softest chromatin belongs to the MCF7 cells, and the MCF10A cells have the most rigid chromatin of all three cell lines. However, at high concentration of Hoechst, the lifetime of the probe in MB-231 cells significantly increases, reaching a value almost as long as the lifetime in MCf10A cells. This increase in lifetime of Hoechst in MB231 cells is attributed to widening of the minor grooves in these cells. Therefore, these results strongly support the hypothesis that chromatin in MB-231 cells is highly deformable. Although not as soft as chromatin in MB-231 cells, Chromatin in MCF7 cells is still softer than chromatin in MCF10A cells. However, since the lifetime of Hoechst in these cells continues to decrease, they are not soft to the extent that their minor grooves can be stretched open at a probe concentration that can stretch the minor grooves of MB-231 cells. Therefore, chromatin in MCF7 cells is not as deformable as chromatin in MB-231 cells. Nevertheless, at much higher concentrations of Hoechst, not studied here, MCF7 chromatin, and even MCF10A chromatin, may be deformable. This is one area of future direction for the comparative study of chromatin softness and deformability and the link to metastatic aggressiveness of tumors. Another potential research direction with implications in therapeutics is to investigate the possibility and the degree to which chromatin softness and deformability are reversible in cells. Treatments such as induced methylation provide a potentially promising area to study whether processes that induce chromatin compaction can reduce or reverse softness and deformability of chromatin in tumor cells, and potentially slowdown the spread of these tumor cells throughout the body.

References

1. Scitable. *Nature Education.* [Online] natuer EDUCATION. [Cited: 02 27, 2021.] https://www.nature.com/scitable/definition/chromatin-182/.

2. Annunziato, Anthony T. Scitable. [Online] Nature Education, 2008. [Cited: 02 28, 2021.] https://www.nature.com/scitable/topicpage/dna-packaging-nucleosomes-and-chromatin-310/.

3. Chrostopher P. Austin. National Human Genome Research Institute. [Online] NIH. [Cited: 02 27, 2021.] https://www.genome.gov/genetics-glossary/Chromatin.

4. Wolfe, A. Chromatin Structure . *Chromatin: Structure and Function.* s.l. : San Diego Academic Press, 1998.

5. Edwige Bano, Louis Fradetal, Maelig Ollivier Ji-Hoon Choi, Valerie Stambouli. SiC Nanowire-Based Transistors for Electrical DNA Detection. *Silicon Carbide Biotechnology.* s.l. : Elsevier, 2016, pp. 261-310.

6. *Free energy analysis and mechanism of base pari stacking in nicked DNA.* Florian Hase, Martin Zacharias. 15, 2016, Nucleic Acid Research, Vol. 44, pp. 7100-7108.

7. Christophe Oguey, Nicolas Foloppe, Brigitte Hartmann. Understaing the sequence-Dependence of DNA Groove Dimensions: Implications for DNA Interaction. [Online] December 29, 2010. [Cited: 05 05, 2010.] https://doi.org/10.1371/journal.pone.0015931.

8. Baylor College of Medicine . Science Daily. [Online] August 2009. [Cited: May 5, 2021.] https://www.sciencedaily.com/releases/2009/07/090713160523.htm.

9. *The Role of DNA Shape in Protein-DNA Recognition.* Remo Rohs, Sean M. West, Alona Sosinsky, Peng Liu, Richard S. Mann, Barry Honig. 461, 2009, Nature, pp. 1248-1253.

10. Luger, J. V. ChodaparambilR. S. EdayathumangalamY. BaoY. -J. ParkK. Nucleosome Structure and Function. *The Histone Code and Beyond.* s.l. : Springer, 2006, pp. 29-46.

11. *Nucleosome Structure and Function.* Robert K. McGinity, Song Tan. 115, 2014, Chemical Reviews, Vol. 6, pp. 2255-2273.

12. *Crystal Structures of Nucleosome Core Particles in Complex with Minor Groove DNA-binding Ligands.* Robert K. Suto, Rajeswari S. Edayathumangalam, Cindy L. White, Christian Melander, Joel M. Gottesfeld, Peter B. Dervan, Karolin Luger. 2, 2003, Journal of Molecular Biology, Vol. 326, pp. 371-380.

13. *Higher-Order Structures of Chromatin:.* Tremethick, David J. 4, 2007, Cell, Vol. 128, pp. 651-654.

14. *EM measurements define the dimensions of the "30-nm" chromatin fiber: Evidence for a compact, interdigitated structure.* Philip J. J. Robinson, Louise Fairall, Van A. T. Huynh, and

Daniela Rhodes. 17, 2006, Proceedings of the National Academy of Sciences of the United States of America, Vol. 103, pp. 6506-6511.

15. *Chromatin Fiber Structure: Morphology, Molecular Determinants,.* Jordanka Zlatanova, Sanford H. Leuba, d Kensal van Holde. 1998, Biophysical Journal, Vol. 74, pp. 2554–2566.

16. *Visualization of early chromosome condensation.* Natashe Kireeva, Margot Lakonishok, Igor Kireev, Tatsuya Hirano, and Andrew S. Belmont. 6, 2004, Journal of Cell Biology, Vol. 166, pp. 775–785.

17. *Regulation of DNA Repair Mechanisms: How the Chromatin Environment Regulates the DNA Damage Response.* Jens Stadler, Holger Richly. 8, 2017, International Journal of Molecular Science, Vol. 18, p. 1715.

18. *Advances in chromatin remodeling and human disease.* Kyoung SangCho, Leah IElizondo, Cornelius FBoerkoel. 3, 2004, Current Opinion in Genetics & Development, Vol. 14, pp. 308-315.

19. *The use of DAPI fluorescence lifetime imaging for investigating chromatin condensation in human chromosomes.* Ana Katrina Estandarte, Stanley Botchway, Christophe Lynch, Mohammed Yusuf and Ian Robinson. 31417, 2016, Scientific Reports, Vol. 6.

20. *Protein phase separation and its role in tumorigenesis.* Shan Jiang, Johan Bourghardt Fagman, Changyan Chen, Simon Alberti, Beidong Liu. 2020, eLife, Vol. 9.

21. *Nuclear Deformation Causes DNA Damage by Increasing Replication Stress.* Pragya Shah, Chad M. Hobson, Svea Cheng, Marshall J. Colville, Matthew J. Paszek, Richard Superfine, Jan Lammerding. 4, 2021, Current Biology, Vol. 31, pp. 753-765.

22. Scitable. [Online] Nature Education. [Cited: May 11, 2021.] https://www.nature.com/scitable/definition/mitosis-cell-division-47/.

23. homas D. Pollard, William C. Earnshaw, Jennifer Lippincott-Schwartz, Graham T. Johnson. Mitosis and Cytokinesis. *Cell Biology.* s.l. : Elsevier, 2017, pp. 755-778.

24. Encyclopædia Britannica. [Online] Encyclopædia Britannica. [Cited: May 11, 2021.] https://www.britannica.com/science/mitosis#/media/1/386154/115447.

25. *Metaphase chromosome structure is.* Ewa Piskadlo, Alexandra Tavares, Raquel A Oliveira. 2017, eLife, Vol. 6.

26. Bio Ninja. [Online] [Cited: May 12, 2021.] https://ib.bioninja.com.au/higher-level/topic-7-nucleic-acids/72-transcription-and-gene/epigenetics.html.

27. Metastatic Cancer: When Cancer Spreads. *National Cancer Institute.* [Online] National Institute of Health. [Cited: May 23, 2021.] https://www.cancer.gov/types/metastatic-cancer.

28. *On the Origin of Cancer Metastasis.* Huysentruyt, Thomas A. Seyfried and Leanne C. 1, s.l. : Critical Reviews in Oncogenesis, Vol. 18.

29. *Evaluation of MCF10A as a Reliable Model for Normal Human Mammary Epithelial Cells.* Ying Qu, Bingchen Han,Yi Yu,Weiwu Yao,Shikha Bose,Beth Y. Karlan,Armando E. Giuliano,Xiaojiang Cui. 7, s.l. : PLOS ONE, 2015, Vol. 10.

30. *Formation of Metastasis by Human Breast Carcinoma Cells (MCF7) in Nude Mice.* Liotta, Samir M. Shafie and Lance A. 2, Bethesda : Cancer Letters, 1980, Vol. 11.

31. *MDA-MB-231 Cell Line Profile.* [PDF] s.l. : European Collection of Authenticated Cell Cultures. 92020424.

32. *Fluorescence lifetime imaging microscopy: fundamentals and advances in instrµmentation, analysis, and applications.* Rupsa Datta, Tiffany M. Heaster, Joe T. Sharick, Amani A. Gillette, Melissa C. Skala. 7, 2020, Journal of Biomedical Optics, Vol. 25.

33. Fluorescence Lifetime Imaging (FLIM). *Picoquant.* [Online] [Cited: May 23, 2021.] https://www.picoquant.com/applications/category/life-science/fluorescence-lifetime-imaging-flim.

34. Jameson, David. Brief Overview of FLuorescence Microscopy. *Introduction to Fluorescence.* s.l. : Taylor and Francis Group, 2014.

35. Two-Photon Excitation (TPE). *Picoquant.* [Online] Picoquant. [Cited: May 25, 2021.] https://www.picoquant.com/applications/category/life-science/two-photon-excitation.

36. *Principles of Two-Photon Excitation Micsocopy and Its Application to Neuroscience.* Karel Svoboda, Ryohei Yasuda. 6, s.l. : Cell, 2006, Vol. 50, pp. 823-839.

37. Michelle Digmand, Enrico Gratton. *The Phasor Approach to Fluorescence Lifetime Imaging: Exploiting Phasor Linear Properties.* [web] Irvine : UC Irvine, 2012.

38. *The Phasor Approach to Fluorescence Lifetime Imaging Analysis.* Michelle Digman, Valeria Caiolfa, Moreno Zamai and Enrico Gratton. 2, s.l. : Boiphysics Juornal, 2008, Vol. 94. 17981902.

39. 14th LFD Workshop. *Laboratory for Fluorescence Dynamics.* [Online] 2019. [Cited: May 25, 2021.] https://www.lfd.uci.edu/workshop/2019/#agenda.